From the Department of Women's and Children's Health
Karolinska Institutet, Stockholm, Sweden

MAGNETIC RESONANCE IMAGING AND ADVANCED IMAGING ASSESSMENT OF THE GROWTH PLATE IN THE ADOLESCENT AND YOUNG ADULT

Ola Kvist

Karolinska Institutet

Stockholm 2022

Published by Karolinska Institutet.
Printed by Universitetsservice US-AB, 2022

ISBN 978-91-8016-802-1
Cover illustration: “Untitled”, mixed media by Ola Kvist 2022

Magnetic resonance imaging of the growth plate in adolescent and young adult

THESIS FOR DOCTORAL DEGREE (Ph.D.)

By

Ola Kvist

The thesis will be defended in public December 2nd 2022, 1 p.m. at Birger & Margareta Blombäck (J3:11), BioClinicum, Karolinska University Hospital.

Principal Supervisor:
Sandra Diaz, M.D., Ph.D., Assoc. Professor
Karolinska Institute
Department of Women's and Children's Health
Division of Paediatric Endocrinology

Co-supervisor(s):
Ola Nilsson M.D., Ph.D., Professor
Örebro University
Department of Medical Sciences
Division of Paediatric Endocrinology

Karolinska Institute
Department of Women's and Children's Health
Division of Paediatric Endocrinology

Carl-Erik Flodmark M.D., Ph.D., Assoc Professor
Lunds University
Department of Clinical Sciences, Malmö
Division of Preventive Paediatrics

Johan Sanmartin Berglund M.D., Ph.D., Professor
Blekinge Institute of Technology
Department of Health

Opponent:
Diego Jaramillo, **M.D.**, **Professor**
Columbia University Medical Center
Department of Radiology
Division of Pediatric Radiology

Examination Board:
Ylva Aurell, M.D., Ph.D., Assoc Professor
University of Gothenburg
Department of Clinical Sciences
Division of Radiology

Seppo Koskinen, M.D., Ph.D., Professor
Karolinska Institute
Department of CLINTEC
Division of Radiology

Per Åstrand, M.D., Ph.D., Assoc. Professor
Karolinska Institute
Department of Women's and Children's Health
Division of Neuropediatrics

Oavsett om man sprättar dynga eller forskar ska man göra det med entusiasm.

- Prof. Gösta Brogren (my grandfather)

"Whether one is doing research or mucking stalls, one should do it with enthusiasm"

POPULAR SCIENCE SUMMARY OF THE THESIS

Imagine a bricklayer building a tower that becomes higher and higher and will be finished once all the bricks have been used. But the tower will not be so high or straight if something happens to the bricklayer or to the tower itself. In the human body the long bones are like the tower and the growth plates are the bricklayer. If something affects the growth plate, for example trauma, then the bone might be crooked or shorter than it otherwise would have been.

The growing bones in child and adolescent skeletal structures have traditionally been evaluated by x-ray. This method looks only at the skeletal portion of the bone and not the growth plate, which is made of cartilage, and cannot be seen with an x-ray. X-ray also involves radiation which in large amounts can cause cancer. The growth plate can also by assessed by tissue sample, a painful method that risks damage to the growth plate itself. Magnetic resonance imaging pictures tissues with free protons i.e., tissues with high water content like cartilage. Magnetic resonance imaging is preferable to the x-ray, which uses radiation, or tissue samples, which are invasive and painful.

Also, of interest is whether magnetic resonance imaging can be used to see "how fast the bricklayer works" by measuring activity in the growth plate. If we can answer this question, we can find premature closure of the growth plate faster than by using an x-ray, and it may have application when considering growth hormone treatment for short stature.

Study I demonstrated that cartilage-dedicated sequence had a greater agreement than T1-weighted sequence and that experience in pediatric radiology increased the agreement.

Study II showed that females mature earlier than males and that being overweight has a modest effect on the skeletal maturity. We found no evidence that physical activity affects skeletal maturity at any location.

Study III showed that MRI performed as well as μCT or histology in an animal model. It also demonstrated that DTI-tractography may be a method to assess activity in the growth plate.

Study IV found that DTI-tractography can be used in a human population together with [insert primary method] to see the maturity of the growth plate and its activity.

POPULÄR VETENSKAPLIG SAMMANFATTNING

Tänk dig en murare som murar ett torn som blir högre och högre. När alla tegelstenar är slut så är tornet klart. Men tornet kommer inte blir rakt eller högt om något händer muraren eller byggstenarna som han ska mura med. I den mänskliga kroppen så motsvarar de långa rörbenen tornen och tillväxtplattorna murarna. Om något skulle hända med tillväxtplattan, till exempel skelettskada, så kanske benet kommer bli snett eller kortare än vad som var tanken.

Det vanligaste sättet att bedöma det växande skelettet hos barn och tonåringar har varit slätröntgen. Slätröntgen avbildar med hjälp av joniserande strålning skelettet och inte tillväxtplattan, som består av brosk. Joniserande strålning kan i stora doser orsaka cancer och ska därför användas så lite som möjligt. Ett annat sätt att se tillväxtplattan är med vävnadsprover (histologi). Detta är både smärtsamt och kan även skada tillväxtplattan. Magnetresonanstomografi (MR) är en metod som avbildar vävnader med högt vatteninnehåll till exempel brosk. Därför borde MR fungera som ett alternativ till slätröntgen, som använder joniserande strålning, eller histologi, som är invasiv och orsakar smärta hos individen.

Det är av intresse att utvärdera om MR kan fungera som ett alternativ metod men också om vi kan se ”hur snabbt muraren arbetar”, dvs mäta tillväxtplattans aktivitet. Om vi kan besvara dessa frågor så bör vi även kunna hitta snabbare och effektivare sätt att bedöma förtidig slutning av tillväxtplattan.

Studie I i denna avhandling visade att brosk-dedicerade sekvenser var lättare att bedöma och att erfarenhet med barnröntgen underlättade.

Studie II visade att flickor mognade tidigare än pojkar och övervikt hade en mindre effekt på den skeletala mognaden. Vi såg inget samband mellan fysisk aktivitet och skeletal mognad.

Studie III visade hos kaniner att MR avbildade tillväxtplattan lika bra som andra metoder, i detta fall µCT och histologi. Studien visade också att DTI-traktografier kan fungera som metod för att bedöma aktiviteten i tillväxtplattan.

Studie IV visade att DTI-traktografier kan fungera som en metod att se mognadsprocessen i tillväxtplattan men även dess aktivitet vilket stämmer med resultatet i studie III

ABSTRACT

The growth plate is a cartilaginous structure located between the metaphysis and epiphysis in long bones. It is the centre for longitudinal growth. Longitudinal growth has a biphasic pattern with a peak during foetal and early postnatal life and another peak during puberty. Growth finally stops after the pubertal growth spurt during late adolescence. Longitudinal bone growth and the skeletal maturation process have traditionally been evaluated with radiographs. MRI has become an alternative since it does not use radiation, visualizes both bone and cartilaginous tissue, and may visualize growth velocity using diffusion tensor imaging (DTI).

The overall aim of this thesis is to investigate how best to image the growth plate and which professionals are most qualified to do the assessment. The following studies were conducted in service of this objective.

Study I: MRI of the knee was performed in 410 individuals and cartilage-dedicated sequences as well as T1-weighted images were obtained. The images were blindly analyzed by general and pediatric radiologists and their observer agreements were compared. Cartilage-dedicated sequence showed greater agreement than T1 and a higher agreement was seen among pediatric radiologists.

Study II: growth plates were imaged at five anatomical sites in 958 individuals using a cartilage dedicated sequence in 1.5 T MRI scanner. The closure of the growth plate was compared to age, sex, pubertal development, BMI and physical activity to see if any of these factors affected the closure of the growth plate. Skeletal maturation occurs in ascending order, from the calcaneus to the distal radius, and correlates with sex, sexual maturation, and BMI but not physical activity.

Study IV: the third study of a human population, this study analyzed DTI of the growth plates of the knee in 159 individuals in a 3 T MRI scanner. The DTI metrics and tractography had a relatively linear relationship with chronological age but a different pattern was seen when the same metrics were compared to skeletal maturation. Tractography was seen in the mature growth plate and should therefore be approached with caution in the later stages of skeletal maturation].

Study III: an animal study performed to validate the results from the previous studies. Twelve rabbits were imaged with MRI, micro computed tomography and histology to compare MRI

with the other modalities. All modalities performed equally well and validated that MRI can be used to assess the growth plate.

In conclusion, the growth plate fuses progressively with age in ascending order and is preferably imaged with a cartilage dedicated sequence and assessed by a pediatric radiologist. The animal model verified that DTI can be used to evaluate the skeletal maturation process and that tractography can be used to assess activity in the growth plate. Tractography seems promising to assess the activity of the open growth plate but must be approached with caution in the later stages of skeletal maturation process of the growth plate.

LIST OF SCIENTIFIC PAPERS

I. Kvist O, Dallora AL, Nilsson O, Anderberg P, Berglund JS, Flodmark CE, et al. Comparison of reliability of magnetic resonance imaging using cartilage and T1-weighted sequences in the assessment of the closure of the growth plates at the knee. Acta Radiol Open. 2020;9(9):2058460120962732.

II. Kvist O, Luiza Dallora A, Nilsson O, Anderberg P, Sanmartin Berglund J, Flodmark CE, et al. A cross-sectional magnetic resonance imaging study of factors influencing growth plate closure in adolescents and young adults. Acta Paediatr. 2020.

III. Kvist O, Damberg P, Dou Z, et al. Magnetic resonance and diffusion tensor imaging of the adolescent rabbit growth plate of the knee. Magn Reson Med. 2022; 1- 12.

IV. Kvist, O, Dorniok T, Berglund JS, et al. DTI assessment of the knee in the adolescent and young adult. *Submitted to Eur J Radiol.*

CONTENTS

LIST OF ABBREVIATIONS

AD	Axonal diffusivity
ADC	Appareant diffusion coefficient
ALARA	As low as reasonable achievable
BAA	Bone age assessment
BMI	Body mass index
BMP	Bone morphogenetic protein
CASAS	Computer-based skeletal age scoring
CASMAS	Computer aided skeletal maturity assessment system
CT	Computed tomography
DTI	Diffusion tensor imaging
DWI	Diffusion weighted imagining
FA	Fractional Anisotropy
FGF	Fibroblast growth factor
FGFR	Fibroblast growth factor receptor
FOV	Field of view
FSE	Fast spin echo
GH	Growth hormone
GP	Greulich and Pyle
GRE	Gradient echo
ICC	Intraclass correlation coefficient
IGF	Insulin-like growth factor
LIX	Readability index (läsbarhetsindex)
MD	Mean diffusivity
NZW	New Zealand white rabbit
PACS	Picture archiving and communication system
PDW	Proton density-weighted
PTHrP	Parathyroid hormone-related peptide
RD	Radial diffusivity
ROI	Region of interest
RUS	Radius, ulna and short bones

SAAS	Swedish age assessment study
T	Tesla
T1W	T1-weighted
T2W	T2-weighted
TE	Time to echo
TGFβ	Transforming growth factor-β
TR	Repition time
TSE	Turbo spin echo
TW	Tanner and Whitehouse
VEGF	Vascular endothelial growth factor
WNT	Wingless/integrated signaling pathway
α	Type I error (alfa)
β	Type II error (beta)
κ	Kappa
μCT	Micro computed tomography
SNR	Signal to noise ratio

1 INTRODUCTION

The concepts of maturity and the transition from childhood to adulthood have been central to society throughout history. *Homo Sapiens* is the "social animal" and maturation—especially sexual maturation—has played an important role in the survival and evolution of the pack [1]. Puberty and sexual maturation are most apparent in females with onset of thelarche and menarche. Environmental factors such as the scarcity of food have had a Darwinistic impact on the age of pubertal onset, especially in females. At the same time, the arrival of menarche could challenge the hierarchy of the pack, resulting in mutiny or the exclusion of the young animal.

With the rise of civilization, increasingly elaborate methods were created to distinguish the transition to adulthood. These can be divided into religious or cultural coming of age rites. The Jewish coming of age tradition of *bar mitzvah* or *bat mitzvah* is a passage according to *Halakha* when a person becomes responsible for their own actions, usually at the age of 13. On the other hand, the Bible states that the age of twenty is the age when one should give offerings to the lord (*Exodus 30:11-16*) and be able to serve in the army, (*Numbers 1:1-3*). Cultural definitions of adulthood are often focused on legal liability, i.e. whether someone is responsible for their actions. The Swedish Criminal Code states that individuals under the age of 15 who have committed crimes cannot be sentenced to any punishment (Ch.6 §6. *Brottsbalken, SFS 1962:700)*. It also states that an individual is fully mature at the age of 21 and sentences should be reduced for those under the age of 21. In fact, the brain is not fully mature until the age of 25 [2]. This has implications from a judicial perspective when an individual is of unknown age. The most common approach in these cases has been to estimate the chronological age has been to evaluate skeletal maturation and the senescence of various growth plates in long bones.

The maturing individual has been an area of interest in the medical field regarding both hormonal and physiological development. For instance, it has been observed that improved childhood conditions of the past 150 years have reduced the age of menarche [3] as well as increased of mean final height at adulthood [4].Some medical conditions, such as precocious puberty, influence both the hormonal and the physiological development. Other medical conditions affect only the bones, more specifically the growth plate, including conditions that cause short stature, dysplasia, osteomyelitis, and Salter-Harris fractures involving the growth plate [5-7].

1.1 SKELETAL MATURATION OF THE GROWTH PLATE

Skeletal maturation and longitudinal bone growth are processes that start in embryo and end after puberty. Endochondral ossification is the main contributor to longitudinal growth in the developing long bones. Endochondral ossification is the process by which the chondrocytes in the growth plate's proliferative zone produce extracellular matrix, which hypertrophies and is gradually replaced by bone. Endochondral ossification is programmed to vary depending on the site, with the most rapid growth in the distal femur [8]. Conditions characterized by slow growth are most prominent in the most active growth plates, for example short femurs seen in achondroplasia.

1.1.1 Morphology of the growth plate

The growth plate cartilage is usually divided into three zones: the resting or reserve zone, the proliferative zone and the hypertrophic zone, which includes the zone of provisional calcification (Figure 1) [9]. The zone furthest from the area of ossification is the resting zone. The chondrocytes here are small and round. Bordering this zone is the proliferative zone. In the proliferative zone the chondrocytes become flattened and arranged in parallel columns [10]. As the chondrocytes enter the hypertrophic zone, they undergo hypertrophy and excrete extracellular matrix which in time becomes mineralized. The cells then die leaving septa for the bone forming structures to invade (osteoblasts, blood vessels and osteoclasts).

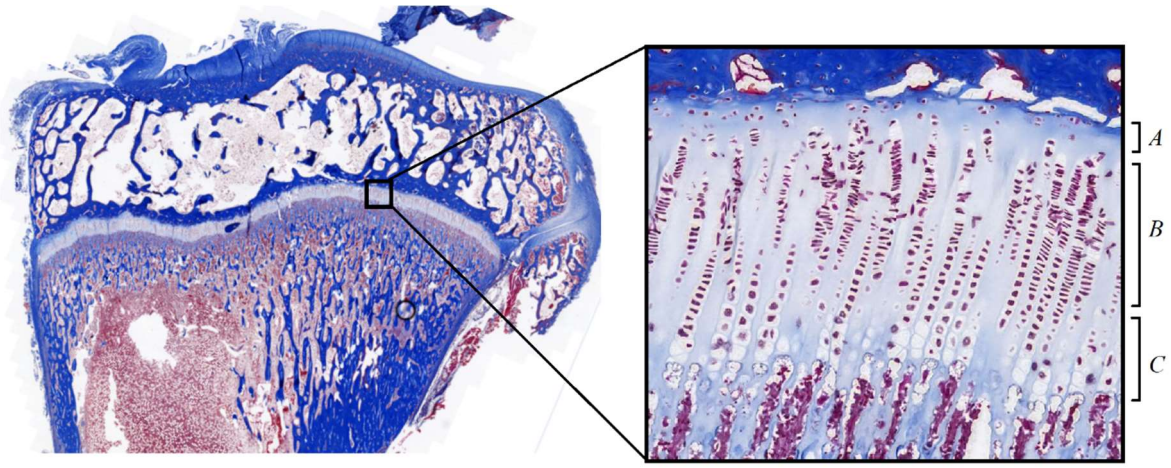

Figure 1. Morphology of growth plate with a Masson's Trichrome stain of the proximal tibia in a 16-week-old New Zealand white rabbit. *A.* The resting zone where the chondrocytes are small, round and scattered. *B.* The proliferative zone where the chondrocytes are flattened and arranged in columns along the long axis of the bone. *C.* The hypertrophic zone where the chondrocytes are enlarged and arranged parallel to the long axis of the bone. (Image from one of the study animals in *Study III* published with consent of Z. Dou.)

1.1.2 Endochondral ossification

Endochondral ossification is a complex process with numerous systemic and local factors affecting the chondrocytes and thus the maturation process that eventually results in complete bone transformation (Figure 2) [11-13]. Growth hormone (GH) is a known systemic factor that regulates the longitudinal growth [14]. The excretion of GH from the anterior pituitary gland into the bloodstream stimulates the liver to synthesize insulin-like growth factor (IGF). This is called the GH-IGF pathway. GH also stimulates the growth plate directly to synthesize IGF1 which in turn stimulates the proliferation of the chondrocytes in the resting zone (Figure 2A). Another factor stimulating longitudinal growth is Indian hedgehog (Ihh), a signaling protein expressed by the pre-hypertrophic chondrocytes close to the proliferative zone that stimulates proliferation and inhibits the hypertrophy of the chondrocytes (Figure 2C). The inhibition of hypertrophy is dependent on the feedback loop that is created with parathyroid hormone-related peptide (PTHrP) [15]. The perichondrial cells expresses PTHrP to promote the proliferation of the chondrocytes (Figure 2B). The PTHrP maintains the chondrocyte in their proliferative state but hypertrophy of the chondrocyte is initiated when the levels of PTHrP drops under a certain level [11]. The proliferative zone is therefore defined by the distance between the site of PTHrP production and the most distant cell [16]. If there is no expression of Ihh, a secondary reduction of PTHrP causes accelerated chondrocyte hypertrophy [17]. A secondary effect is that Ihh is part of the osteoblast formation in the periosteum. St. Jaques et al. concluded that Ihh is needed to sustain the expression of PTHrP and to control the chondrocyte maturation [17].

Bone morphogenetic factors (BMP) belong to the transforming growth factor-β (TGFβ) family and induce skeletogenesis, including initiation of chondrogenesis without Ihh [11]. The proliferative chondrocytes express BMP7 whereas the pre-hypertrophic and hypertrophic chondrocytes express BMP6. BMP7 promotes cell proliferation and collagen type II synthesis while BMP6 stimulates the IHH expression to promote chondrocyte hypertrophy [18]. The BMP signal induces Ihh expression by the chondrocytes. It has been documented that BMP works parallel to the IHH-PTHrP pathway to maintain a normal chondrocyte proliferation [19]. Similarly, the effects of Ihh on the proliferation of chondrocytes are independent of BMP [20]. BMP6 and BMP 7 would seem to have minor influence on longitudinal growth since it has been demonstrated that mice lacking BMP6 or BMP 7 nevertheless exhibit normal bone growth [21, 22].

Fibroblast growth factors (FGF) consist of 22 distinct genes and four fibroblastic growth factor receptor (FGFR) genes. The FGF genes can be grouped into six subgroups with sequence similarities [23]. FGFR1 and FGF7, FGF8 and FGF10 are needed to initiate limb budding.

Later, FGFR2 is expressed in the mesenchymal condensation as well as in the periosteal cells and in osteoblasts. Each zone in the growth plate has their FGFR expression with little overlap. In the resting zone low levels of FGFR2 are expressed, in the proliferative zone high levels of FGFR3 are expressed, and high levels of FGFR1 are found in the pre-hypertrophic zone and hypertrophic zones [23]. Of these receptors, FGFR3 is best understood, and it is FGFR3 that affects the proliferative chondrocytes and their development into pre-hypertrophic and hypertrophic chondrocytes [24]. A study with knockout of FGFR3 in mice showed an expansion of the length of chondrocyte columns as well as an increase of chondrocyte proliferation [24]. It has also been demonstrated that there is an inverse relationship between FGFR3 and Ihh; an activation of FGFR3 decreases Ihh expression and vice versa [23]. It has also been demonstrated that mutations in FGFR3 cause short-limbed dysplasias in humans, such as achondroplasia [25, 26].

Wingless/integrated (Wnt) is a diverse family of lipid-modified signaling glycoproteins with two different pathways that are either β-catenin dependent (canonical) or β-catenin independent (non-canonical) [27]. The canonical pathway is involved in the transformation of mesenchymal cells towards chondro- and osteogenesis and is later involved in regulating the chondroprogenitor cells in the growth plate [13]. The Wnt signaling pathway stimulates chondroprogenitors in the resting zone (Figure 2A) as well as in the outermost layer of the growth plate, promoting appositional growth [28].

Vascular endothelial growth factor (VEGF) regulates angiogenesis by inducing proliferation and migration of endothelial cells (Figure 2D). VEGF functions as survival factor for chondrocytes in hypoxic regions and its expression by hypertrophic chondrocytes is crucial for the transformation into bone [29]. The expression of VEGF from the hypertrophic chondrocytes promotes vascular invasion into the growth plate. This process is regulated by *Runx2* [30-32]. A secondary effect of VEGF is that is the vascular invasion is needed for the osteoclasts; VEGF is therefore part of angiogenesis as well as osteoclast regulation [33].

Mutations of the different pathways in the endochondral ossification can result in various dysplasias. For example, mutations of the FGFR3 gene express on a spectrum from milder hypochondroplasia to lethal thanatophoric dysplasia [23]. An early and correct diagnosis of the affected pathway can be crucial since treatments are emerging to treat or reduce the severity of various congenital syndromes.

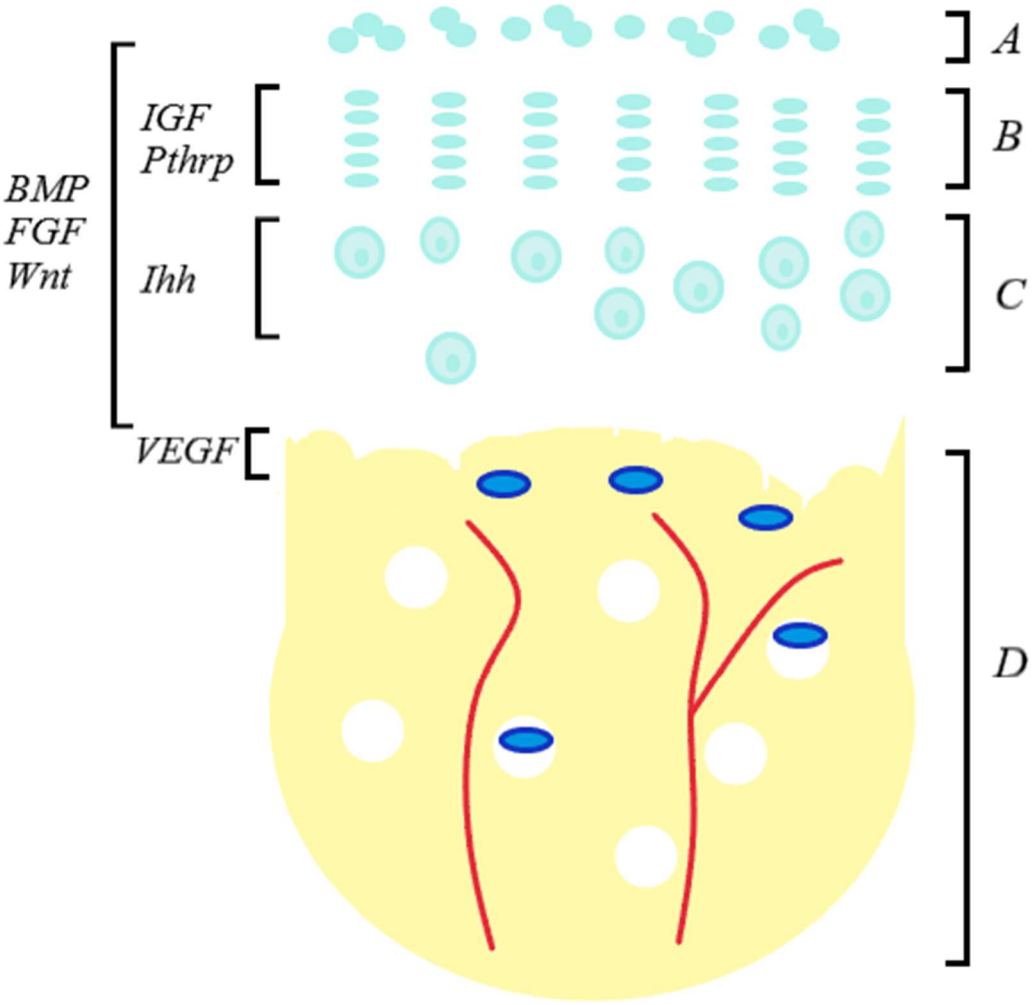

Figure 2. Endochondral ossification

A. Resting zone: IGF1 stimulates the chondrocytes in the resting zone to proliferate.

B. Proliferative zone: PTHrP promotes the proliferation of the chondrocytes and a low level of PTHrP causes the cells to undergo hypertrophy. BMP supports the proliferation of chondrocytes and BMP7 is expressed by proliferative chondrocytes. FGFR3 inhibits chondrocyte proliferation and accelerates their hypertrophy

C. Pre-hypertrophic zone: Ihh is expressed by the pre-hypertrophic chondrocytes close to the proliferative zone to inhibit the hypertrophy of the chondrocytes. Hypertrophic zone: BMP is required for the hypertrophic differentiation. VEGF promotes vascular invasion into the growth plate

D. Metaphysis: VEGF causes angiogenesis and regulates osteoclasts.

2 LITERATURE REVIEW

2.1 RADIOGRAPH

Radiology has long been used to assess the skeleton ever since its invention by Wilhelm Conrad Röntgen. The radiograph technique depicts the mineralized parts of the skeleton which makes it especially useful for the detection of fractures. However, radiographs do not depict the soft tissues of the growth plate but only the mineralized metaphysis, epiphysis, and—in the late stage of skeletal maturity—the final stages of skeletal maturation when the growth plate has completely transformed into bone. Studies have been made to develop atlases of the ordinary skeletal maturation process. The most commonly recognized atlas is by Greulich and Pyle (GP) [34], on the basis of a study performed between 1931 and 1942 as part of the Brush Foundation Study of Child Growth and Development. The population consisted of socio-economically middleclass children in Cleveland, Ohio, examined at intervals of 3 to 12 months during the study period. The most famous atlas is of the left hand but Pyle et al. also created an atlas of the knee [35]. The results of these studies created an estimation of the bone appearance for both sexes at certain ages, thence referred to as the bone age. The GP method compares a radiograph of the bones of the hand with the GP-atlas to make a bone age assessment (BAA). Another famous atlas is by Tanner-Whitehouse (TW), developed from left wrist and hand radiograph of children in the UK between 1950 and 1960. The updated TW2 was published in 1983 [36], based on a study population of children of average socioeconomic class, was subsequently updated and re-published in 2001 as the TW3 [37]. The TW3 method assess the distal radius, ulna, and short bones (RUS) of the first, third and fifth phalanx, as well as the seven carpal bones. Each bone is compared to an atlas and scored with regard to the maturity and sex of the individual. The different scores are then averaged to an estimated bone age.

One disadvantage of these methods is that manual assessment is time-consuming and prone to inter- and intra-rater variability. Therefore, several automated approaches to BAA have been developed to exclude the human observer. Most of these methods assess the skeletal maturation process of the bones in the left hand and wrist. The first semi-automated system for BAA was presented in 1989 [38]. The CASAS (Computer-based skeletal age scoring) system introduced in 1994 was a semi-automated system with BAA based on the TW2 method and using an overlay pattern [39]. The system rated 13 different bones (radius, ulna, the metacarpals, and the phalanxes of the first, thirds and fifth finger). A more automated system called CASMAS (computer aided skeletal maturity assessment system) was introduced 1999, also based on

TW2.This system classified the middle phalanx of the hand in Japanese children aged between 2-15 years old to assess their bone age [40].

Further development of artificial intelligence and neural networks has resulted in more advanced systems to analyze BAA. Liu et al. developed an artificial neural network that estimated the BAA on two geometric features of the RUS and the carpals [41], while Hill et al. created ROHSAS (The Royal Orthopedic Hospital Skeletal Ageing system), a 13- and 20-bone assessment based on the TW2 method [42]. The latter system finds the outline of the hand and its bones and estimates the BAA within 4 minutes. In 2009, the BoneXpert system was introduced as an automated method for BAA (Figure 3) [43]. This system relies primarily on the TW approach and shows a standard deviation of 0.42 years compared to GP and 0.80 years compared to TW. This software has been further developed and is now considered a reliable method for BAA in patients with short stature [44] and tall stature [45].

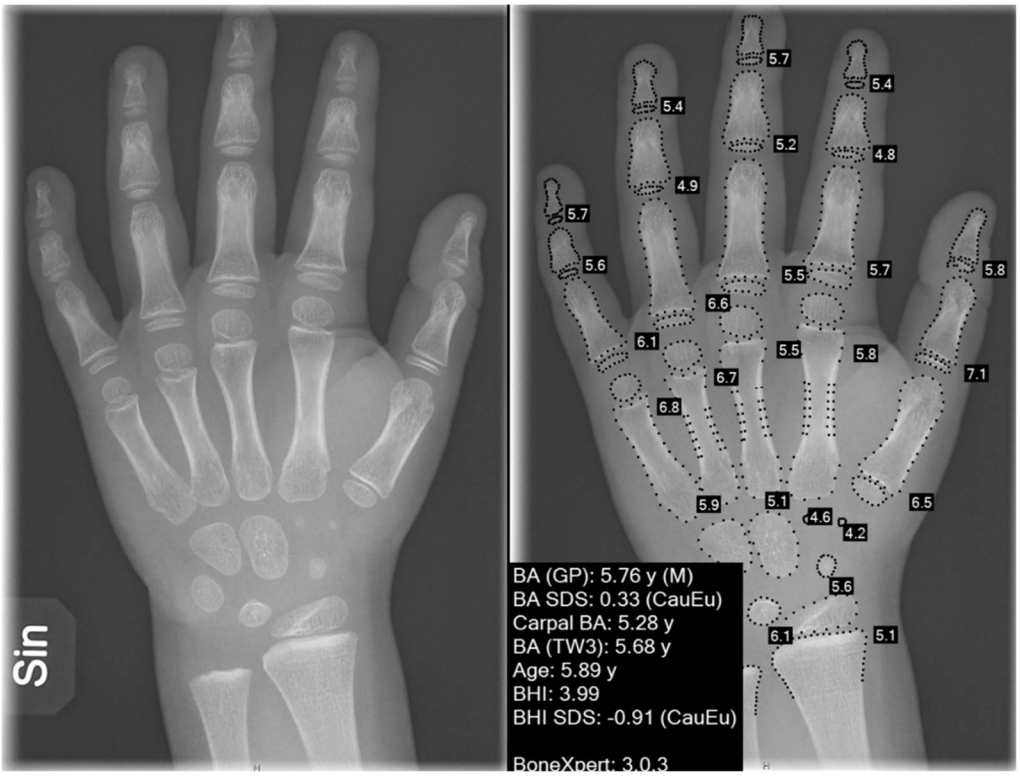

Figure 3. A frontal view of the left hand and wrist in a six-year-old child. The BoneXpert algorithm locates the borders of the different bones and assigns a GP bone age to each individual bone, 21 total. The average score is then reported as *BA (GP)*. Similar procedure is done but the TW3 age is assigned to each bone and averaged. The chronological age of the individual is reported as *Age.* (Images printed with consent from the patient and their legal guardian)

From a medical standpoint, BAA is of interest in various orthopedic disorders, in pediatric endocrinology, and as a tool to project a developing individual's likely final height [46]. In more recent years, bone age has been an area of interest in forensic medicine to assess whether an individual without verified date of birth is a minor. In the European judicial system there are multiple age thresholds with implications for penal law and the right to asylum, including the 14th, 16th, 18th and 21st years of life [47].

2.2 COMPUTED TOMOGRAPHY

Radiographs of the hand and wrist are considered a reliable method for BAA in individuals up to age of 18 in females and 19 in males [48]. In forensic medicine there is a further need to determine if an individual of unknown age is older than 21 years, mainly because in differences in sentencing in penal law. The medial epiphysis of the clavicle is the best region for analysis in that age-group [49-51]. Studies of the medial clavicle have been done with radiograph [49], but computed tomography (CT) with its possibility of multiplanar reconstructions is considered the imaging modality of choice [50]. Initial radiograph-based studies of the medial epiphysis of the clavicle categorized the skeletal maturation process in four stages:

Stage 1: nonunion without ossification of the epiphysis.

Stage 2: nonunion but with ossification of the epiphysis.

Stage 3: partial union of the ossified epiphysis and metaphysis.

Stage 4: complete union of the ossified epiphysis and the metaphysis [52, 53].

Schmeling et al. studied the medial clavicle with CT and subdivided stage 4 (Stage 4: complete union of the ossified epiphysis and the metaphysis, visible epiphyseal scar; stage 5: complete union of the ossified epiphysis and the metaphysis, no visible epiphyseal scar) [49, 54].

Kellinghaus et al. added further subgroups to better describe the skeletal maturation process, pertaining to both the ossification of the epiphysis in comparison to the metaphyseal ending as well as the fusion of the growth plate. They added the subgroups "*a, b and c*" to stages 2 and 3 [55].

One consideration with regard to non-medical examinations is the ALARA (as low as reasonably achievable) principle. According to ALARA, examinations must be beneficial to the individual examined. Retrospective studies have been made to evaluate if low-dose CT in

medical exams can be used to evaluate the skeletal maturation process of the clavicle [56]. The method to assess the growth plate of the medial epiphysis of the clavicle was developed in Germany and has been of interest in Turkey (in the context of migration to Europe from the Middle East) and Asian countries (to compare populations of Asian and European heritage) [57-59]. Each system has its own strengths and weaknesses. Systems with fewer stages are easier to use and should result in lower inter- and intra-rater variability, but the specificity of each stage is not as high.

2.3 MAGNETIC RESONANCE IMAGING (MRI)

The methods to evaluate skeletal maturity mentioned above entail assessment of the bones as opposed to the cartilaginous growth plate, the active site of endochondral ossification and longitudinal bone growth. Radiography and CT use ionizing radiation which should be avoided as much as possible, as formalized by the 2013/59/EURATOM directive emphasizing the imperative to regulate and reduce the use of ionizing radiation for non-medical purposes, including forensic medicine [60]. MRI measures the density of hydrogen protons i.e., water, in the tissues of the body and various MRI sequences enhance different properties of a tissue. MRI is commonly used in clinical practice to evaluate articular cartilage, as cartilage has a high-water content and is therefore conducive to MRI. Accordingly, the growth plate has a high signal on T2-weighted (T2W) sequences. T1-weighted (T1W) sequences primarily enhance fat whereby the growth plate has an intermediate signal on T1W images. Other MRI sequences have been developed to further enhance the signal of cartilaginous structures [61, 62]. The water content of the growth plate has been verified by physical assessment in animal studies [63]. The question of which growth plate is most suitable for age assessments and various technical aspects have been topics of discussion in this context.

2.4 BODY PART

Various studies have been done to estimate the skeletal maturation process in different parts of the body, mainly from a medicolegal perspective to ascertain if individuals are older than 18, or in some instances 21 years old. The accuracy of forensic age estimations and methodologies are subject to debate, especially with regard to statistical calculation [64, 65]. Anatomical locations and their growth plates are of not of equal importance with regard to age estimation [66]. The reference standard is still considered to be GP and TW and their radiographs of the wrist and hand. Thodberg et al. found this method to be reliable for females under the age of 18 and males under the age of 19 [48].

2.4.1 Radius

Multiple studies have assessed the skeletal maturation process of the wrist and the distal radius in particular [67-76]. These studies have identified stages of the skeletal maturation process of the growth plate where the end stage is that the growth plate is no longer visible (Figure 4). Some studies have used a simplified three-stage system to improve intra- and inter-rater agreement and reduce subjective errors [70]. Other studies have used an adapted version of an older grading scale from radiograph and/or CT studies [68, 71]. Dvorak et al. introduced a six stage system as well as the term residual physis, which had not been mentioned in earlier studies using ionizing radiation [77]. Issues raised by these studies include differences between bone age and chronological age relating to the ethnicity and/or socioeconomic status of the participants.

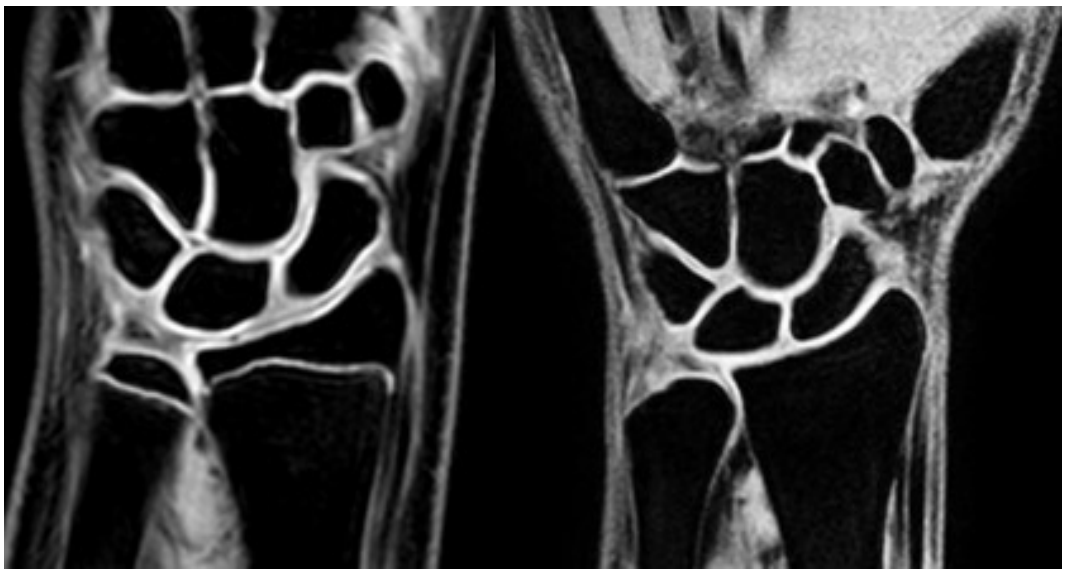

Figure 4. Cartilage dedicated sequence merged fast field echo (mFFE) of the left wrist on a 1.5 T Philips scanner. The growth plate has a high signal due to the high-water content and is open (left image). On the right image the growth plate has completely fused (both ulna and radius) and only the articular cartilage has a high signal. (Images reprinted with consent from the individuals)

2.4.2 Knee

Studies of the knee have developed different grading scales based on the atlas by Pyle et al [35]. The most basic scale is a three stage system developed by Jopp et al. [78] Dedouit et al. created their own five stage system but also noticed that on radiographs the growth plate could appear completely fused, unlike on MRI [79]. This preliminary study concluded that MRI could be used to assess skeletal maturity i.e., bone age. Krämer et al. repeated this study using a modified staging scale based on the grading scales of Schmeling et al. [49] and Kellinghaus et al [55, 80, 81]. The results of these studies are not comparable since Krämer et al. used T1W images and Dedouit used proton density weighted (PDW) images. To address this, Saint-Martin et al. (all-male study population) and Ottow et al. (both genders) repeated the study by Kramer et al., which resulted in similar results and concluded that the differing results of the Schmeling and Kellinghaus studies were due to the choice of MRI sequence [82, 83]. Vieth et al., on the other hand, created a grading scale of the growth plate in a prospective study that included both T1W and T2W images [84]. The purpose of the study was to evaluate the growth plate in a more traditional matter (T1W) but also to consider the watery components of the growth plate with T2W images. The study was later repeated using routine examinations, both 1.5 T and 3.0 T scanners, with ordinary T1W and T2W images [85]. Another approach to validate MRI was a comparative study between radiograph and MRI that showed a good correlation between chronological age and grading of skeletal maturation [86]. Surprisingly, this study found that MRI had a relatively higher R-square than radiographs. These results indicate that imaging of the cartilaginous growth plate combined with slice analysis gives more information about skeletal maturity than a summarized image i.e., a radiograph.

Researchers have also sought to determine whether growth plate fusion has a uniform or non-uniform pattern. The results vary since non-uniform patterns with closure starting centrally in the femur [87] as well as a uniform patterns have been reported [88]. Residual physes have been described as remnants in the anterior and posterior portions of the fused growth plate on T1W images (Figure 5) [77]. The residual physes on T1W images imply that growth plate fusion has a centrifugal pattern. A Turkish study is of particular interest, since they have conducted MRI studies of the knee according to both the study protocol by Dedouit et al.[79] in 2016 [89], as well as according to Krämer et al. in 2020 [80, 81, 90]. Unfortunately, the latter study contains no discussion of which protocol is preferred.

Figure 5. In the anterior portion of the femoral growth plate there is a thick black line (white arrow) on T1W indicating a residual physis according to Dvorak et al [67]. (The image of a volunteer from *Study I* is reprinted with consent SAGE journals.)

2.4.3 Ankle

There is anatomical variety in the skeletal maturity process of the calcaneus. The number of secondary ossification centers varies, and up to 44% of individuals have multiple ossification centers [91]. This feature can complicate the assessment of the skeletal maturation process, as can various medical conditions. Saint-martin developed a three-stage system in 2013 based on epiphyseal-metaphyseal fusion in the distal tibia and calcaneus [92]. The above-mentioned complicating factors explain why their scale only has three stages, but it also ensures a significant result and high observer agreement. Stage 3 was seen at the earliest at the age of 12 years in females and age of 17 years in males. A Turkish study using the same sequence and staging scale observed stage 3 at 14 years in females and 15 years in males [93]. They concluded that a different standard of living in the study populations might account for the differences in skeletal maturation observed in the two studies.

2.4.4 Clavicle

The clavicle has some unique features regarding skeletal maturation. First, it has initially membranous ossification and later endochondral ossification, wherein the medial ossification center appears during adolescence [50, 94]. Studies were made first with radiograph and later with CT [49, 55, 57, 58, 95, 96]. These studies have determined that the overlap of structures in the medial clavicle on a radiograph makes CT preferable, despite the increased exposure to ionizing radiation. The imperative to reduce ionizing radiation according to the ALARA principle has resulted in efforts to create low dose protocols [56] and radiation-free methods like MRI [97-101]. The assessment of the medial clavicle can be a complicated procedure given the presence of normal variants [96].

2.5 AUTOMATED METHODS

The 2013/59/EURATOM directive introduced for regulation of non-medical exposure to radiation[60]. This identified the need for an MRI atlas along the lines of GP and TW as well as an automated method like BoneXpert. Auf der Mauer et al. performed a prospective study with a two-year follow up, in which they performed MRI of the knee and evaluated skeletal maturity using a three-stage scale [102]. They identified earlier onset of ossification in the tibial growth plate compared to the distal femur. The tibial growth plate also had a slower and steadier pace of skeletal maturation compared to the femoral growth plate. These findings are of special interest for the creation of an MRI atlas.

Pennock et al. used 859 MRIs of the knee (421 females and 438 males aged between 2 -19 years) to create an atlas (including patella, fibula, tibia and femur) [103]. Referral images were based on age and sex. The atlas was validated by a follow up of 321 MRI compared with chronological age and bone age estimation from hand radiograph. The study concluded that the patella provided the best age assessment in early childhood, while the tibia was preferred in later childhood. In 2018 Pröve et al. created an automated segmentation of the knee using convolutional neural network [104]. On the basis of 76 datasets (males aged between 14 and 20 years), they created a training set, validation set and test set. The chosen model for the neural network was a combined model that evaluated the femur, tibia, and fibula in a merged assessment. The first run of the training set produced a Kappa (κ) of 0.753, which after 40 epochs had increased to 0.981 with similar results in both the validation and test set. These results were later validated in a larger population and published in 2021 [105]. Similar studies in the field of automated age estimations on MRI have been made by Dallora et al. [106], also of the knee, and Stern et al. focused on the hand [107, 108].

2.6 TECHNICAL ASPECTS

2.6.1 Field strength

The field strength of the MR-scanner is a technical aspect that may have affected the results of the aforementioned MRI studies. In short, the stronger the field, the stronger the signal. Most studies have used either a 1.5 T or a 3 T whole-body MR-scanner. Wong et al. performed a study imaging the same patients on both 1.5 and 3 T comparing image quality and visualization of cartilage pathology [109]. As expected, radiologists found it easier to visualize anatomical structures and abnormalities on 3 T in comparison to 1.5 T. Naturally, 3 T had a higher signal to noise ratio (SNR) because of the higher magnetic field i.e., the field strength. A comparative study has also been performed to assess the difference between a 1.5 T whole-body MR-scanner and a dedicated extremity MR-scanner [110]. The study concluded that a whole-body scanner has better image quality (especially with regard to fat suppression) and faster examination time. However, the extremity scanner was less noisy.

2.6.2 Choice of sequence

Most studies have been based on a single sequence. The majority of studies have used T1W images [67-71, 77, 80-83, 86, 90, 92, 102, 111], and to lesser extent PDW [75, 79, 112] or T2W/T2*W [88, 89]. Only a handful of studies have been performed with a combination of T1W and T2W or cartilage dedicated sequences [84, 85, 91, 113, 114]. An advantage of using two different sequences is that they emphasize different properties in soft tissues which can yield different results and stagings. For instance, early bone bridging is easier to see on T2W images than T1W because of the high signal in the growth plate. On the other hand, T1W images are superior to visualize sclerotic remnants of the growth plate.

2.6.3 Diffusion

More experimental studies have focused on the histological and physiological properties of the growth plate. The random Brownian motion of water molecules in a tissue can be measured with diffusion weighted imaging (DWI). On DWI images restricted diffusion is bright white but tissues with high T2 signal are also bright. This is called T2 shine-through. To avoid misinterpreting the apparent diffusion coefficient (ADC) can be calculated by subtracting the image with high *B*-value from the *B0* image. Therefore, an object with restricted diffusion will have a bright signal on DWI and low signal on ADC while T2 shine-through will have a high signal on both images. ADC of the growth plates of the knee have been studied in adolescent soccer players [112]. To further investigate diffusion one can use diffusion tensor imaging (DTI). DTI measures diffusion in a number of directions to assess if the diffusion spherical or

more ellipsoid [115]. This gives more detailed information regarding tissue structure, with the main measurement called fractional anisotropy (FA). FA value is a scalar value between zero and one. Zero means that the diffusion is isotopic (spherical), and one means that the diffusion is fully restricted in every direction except for one. The shape of the diffusion is calculated by three so called eigenvalues. The eigenvalues represent the three semi-axes of a sphere used to calculate whether the diffusion is spherical or cigar shaped. Other measurements that can be acquired from DTI are mean diffusivity (MD), axial diffusivity (AD), and radial diffusivity (RD) as well as tractography measurements [116]. The MD is the average sum of all three eigenvalues, roughly equivalent to ADC. Axial diffusivity (AD) is consists solely of the parallel and largest eigenvalue, whereas radial diffusivity (RD) is the average of the two smaller eigenvalues [115]. From the region of interest (ROI) one can perform a tractography, a.k.a. fiber tract reconstruction. Tractography is a 3D reconstruction technique that was developed to analyze neural tracts in the CNS [117]. To perform tractography one needs to enter a minimum FA value threshold and a maximum turning angle to filter to create a framework of what is considered a tract and a criterium for its endpoint. The tractography analyzes the diffusion tensor voxel-by-voxel creating a fiber whose size and orientation is relative to the above-mentioned criteria.

Studies have assessed anisotropy in the diffusion of water in the growth plate [118-123]. These studies hypothesized that parallel columns of chondrocytes in the proliferative zone cause anisotropy and thus DTI can be used as biomarker regarding growth velocity, especially tract volume [119]. A study in a larger cohort found that the ADC-value peaked before the peak-velocity growth spurt while tract length and volume were more pronounced at the expected age of peak-velocity growth. The conclusion was that diffusion parameters and tract length seem to be influenced by age and differences between the femur and the tibia [124]. High resolution DTI studies of articular cartilage biopsies have yielded further insights. Examinations done on high field MRI scanners (8.45 – 17.6 T) found that the largest eigenvalue had a distinct zonal pattern similar to the collagen network with a tangential orientation centrally and radial orientation in proximity to the articular surface and the resting zone [125-127]. Another finding was that cartilage had weak anisotropy with an estimated FA value between 0.1 – 0.2. The low FA value means that all future studies need high accuracy to eliminate confounders caused by background noise [126]. Animal studies taking histological samples are needed to validate the assumptions that tract length and volume is larger during the growth spurt.

2.7 ANIMAL STUDIES

Animal models with similar bone growth to humans are suitable for studies relating to skeletal maturity. Rabbits are one of the smallest mammals that have a skeletal maturity that correlates with puberty (unlike smaller animals like mice and rats) [128, 129]. Specific traits of various rabbit species have been evaluated and compared to humans to map their use as study animals, including the relation between rabbit age and human age [130]. One of the most common ways to depict skeletal maturity in animal models has been through micro computed tomography (μCT) [131], which is a high-resolution version of CT with an effective pixel size smaller than 1.1 μm [132]. μCT is excellent at detecting early bone-bridging but is not optimal to study the cartilaginous growth plate. Other animal studies of cartilage have focused on MRI and histological comparison. It has been demonstrated that MRI can monitor injuries of the growth plate in a rabbit model by comparing MRI (T2W, PDW and DWI), μCT and histological samples [133, 134]. Similarly, the porcine growth plates of the proximal tibia and proximal femur have been evaluated with both ordinary MRI sequences (T1W, T2W and PDW) [135] and diffusion tensor[136]. The pigs in the study by Shiguetomi-Medina et al. were of unknown age and therefore hard to correlate to human skeletal development. Other animal studies performed with DTI have imaged the growth plate of the knee in rats and factors affecting its various anisotropic properties [137, 138]. Unfortunately, studies using rodents offer limited insight to the human as rodents' skeletal maturity is unrelated to puberty [128]. Conversely, rodents have an open growth plate and therefore have longitudinal growth throughout life [129]. Studies of the articular cartilage in bovine [139], porcine [140] and well as in rodent models [137, 138] have further assessed DTI properties in cartilaginous structures, and how different settings may affect results [137, 138].

2.8 FACTORS AFFECTING SKELETAL MATURITY

The most common factors discussed in relation to skeletal maturity are age, sex, hormones (including sexual maturity), physical activity, ethnicity, and socioeconomic status. There is a known difference of mean chronological age between females and males regarding the skeletal maturation process. In clinical settings, the stages of puberty from onset to full sexual maturity are assessed by pediatricians on the five-stage system of secondary sexual characteristics developed by Marshall and Tanner [141, 142]. The role of assessment by a pediatrician vis-à-vis self-assessment may not be of critical importance, since Chavarro et al. did not record significant differences in the assessment of pubic hair growth, for example, although males tended to overrate their genitalia staging [143].

2.8.1 Socioeconomical

The availability of food, risk of infection and predation are known environmental factors that have had a Darwinist effect on sexual maturation and the skeletal maturation process. These factors are not strictly connected but anthropological studies of menarche have found it probable that skeletal maturation has changed throughout human history. The time of menarche seems to have fluctuated with from between 7 - 13 years of age for the Paleolithic woman [144], to 12 -15 years for the Medieval woman, and 15 - 16 years of age during the 19th century (15 to 16 years of age) [3]. One theory is that this was a result of poorer nutrition and increase of infectious diseases since the Paleolithic era. Similarly, the improved nutrition and management of infectious diseases during the 20th century has reduced the age when menarche occurs, especially in the developed countries where it now seems to slow down or level off with onset of menarche at 12 to 13 years of age. Various studies have found that ethnic origin and socioeconomic status influence the skeletal maturation process and the corresponding relationship between bone age and chronological age [54, 57, 67, 77]. Epidemiological studies show that populations are generally taller today than previous generations. For example, Iranian men born in 1996 are 16.5 cm taller than those born 1896 [145]. However, the same study also found no evident increase of adult height in parts of South Asia as well as in some sub-Saharan African countries during the same time period. The improved socioeconomical situation have also caused an increase of conditions related to surplus of food e.g., obesity. A survey study conducted in western Sweden in 2008 among 15-year-olds had a population that contained 15.1% overweight and 3.0% obese males and 9.9% overweight and 1.9% obese females [146]. The association between obesity and advanced skeletal maturity has been reported both in prepubertal children [147] and in adolescents [148-150]. In summary, increased of standard of

living results in earlier occurrence of menarche and taller final height, which suggests an inverted relationship between these two occurrences.

2.8.2 Hormonal

Estrogens are a group of hormones involved in normal sexual development in females including thelarche. It has been documented that estrogen accelerates the skeletal maturation process including growth plate fusion [151]. Further analysis noted an accelerated decline of progenitor cells in the resting zone caused by estrogen, which could be one of the mechanisms that accelerate growth plate senescence [152]. Estrogen levels can be linked to obesity since adipose tissue has an endocrine function that synthesizes aromatase which converts androgens to estrogen. The earlier onset of menarche in overweight females as compared to underweight is likely linked to estrogen synthesized by adipose tissue [153]. Another consideration is that increased amounts of adipose tissue cause insulin resistance and an increase of insulin-like growth factor (IGF-1), which is connected to growth hormone (GH) [154]. These hormones play a key role in puberty and the growth spurt, and it has been documented that the average weight of American girls increased from the late 1970s to the early 1990s [155]. Various studies have been made of the hormonal aspect of obesity, especially androgens like dehydroepiandrosterone sulfate (DHEAS) [147, 156] and IGF-1 [157, 158]. Most studies agree that levels of DHEAS correlate with advanced bone age, but results have been more contradictory regarding IGF-1. It is worth noting that some studies have not corrected for the possible confounding effect of sex hormones [156]. While obesity affects the height of children and the onset of puberty, there does not seem to be an association between weight and final height [159].

2.8.3 Physical activity

The impact of physical activity on skeletal maturity is still unclear. A review of literature observed that male elite soccer players seem to be more skeletally mature than their peers, while the reverse is true of female gymnasts [160]. Further studies have been performed to compare the growth plate of gymnasts to their peers to see if one can detect changes in the cartilage before they develop gymnast wrist [76]. The widened growth plate has been described as result of stress fracture that causes hypertrophied cells to fail to ossify [134, 161]. The widened growth plate can result in a lower staging of skeletal maturation. Studies by FIFA have raised questions whether socioeconomic factors have an impact, or whether observations of advanced skeletal maturity may be related to age doping [67, 77]. Other discussions in forensic medicine have taken up the potential impact of socioeconomic status, selection bias among youth elite athletes, and exogenous anabolic steroid use on skeletal maturity [162, 163].

Müller et al. showed that a large portion of elite athletes in Austria (ski racers and soccer players) were born in the first months of the year which could be a result of selection bias due to physical development compared to their peers born later the same year [164]. Other MRI studies have shown ADC and DWI measurements of adolescent football players that imply higher cellularity in the medial tibial growth plate. The higher cellularity was considered an effect of varus angulation of the knee and a higher mechanical load in comparison to the lateral growth plate [112].

3 AIMS OF THE THESIS

The overall aim of this thesis is to appraise the use of MRI and increase the knowledge regarding growth plate appearance and maturation in the adolescent and young adult. The specific aims of each paper are:

I. *How to image the growth plate?*
To compare two different MRI-sequences, cartilage dedicated sequence compared to bone-dedicated sequence; to assess the growth plate development.

II. *How does the growth plate mature?*
To investigate the relationship between chronological age, BMI and development/fusion of growth plates at five different locations (radius, distal femur, proximal and distal tibia and calcaneus) using MRI with cartilage-dedicated sequence.

III. *How do we confirm MRI findings using advanced technique including diffusion tensor (DTI) and tractography?*
To assess the growth plate with MRI including DTI and tractography in an animal model and evaluate if there is are significant differences with regard to μCT or histology.

IV. *Can MRI see the activity in the growth plate in humans?*
To evaluate the growth plate and the feasibility of MRI-DTI-tractography in a healthy young population to assess the maturity of the growth plate.

4 OVERVIEW RESEARCH QUESTIONS

Figure 6. Overview of the research questions by study.

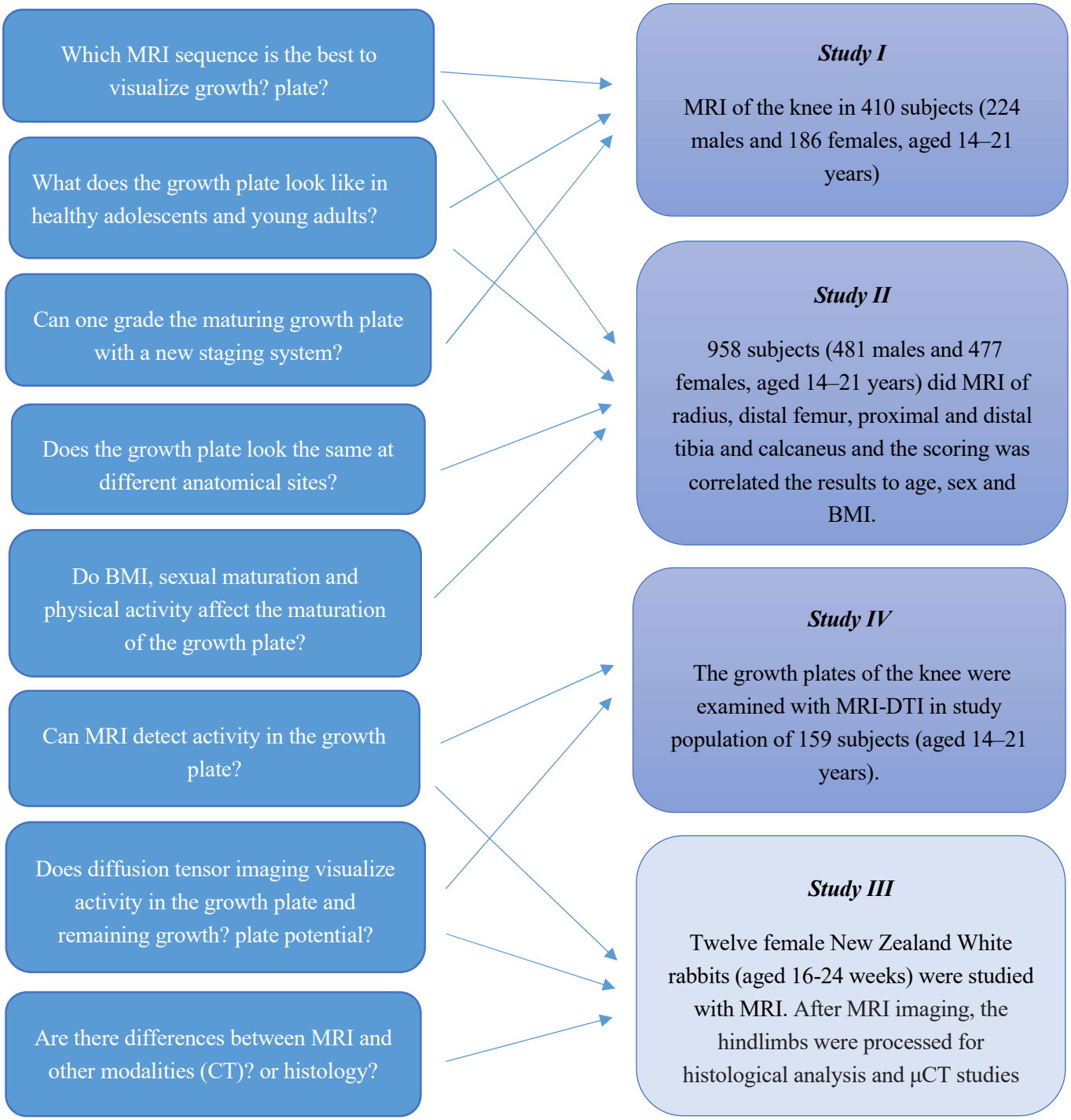

5 MATERIALS AND METHODS

5.1 STUDY POPULATIONS

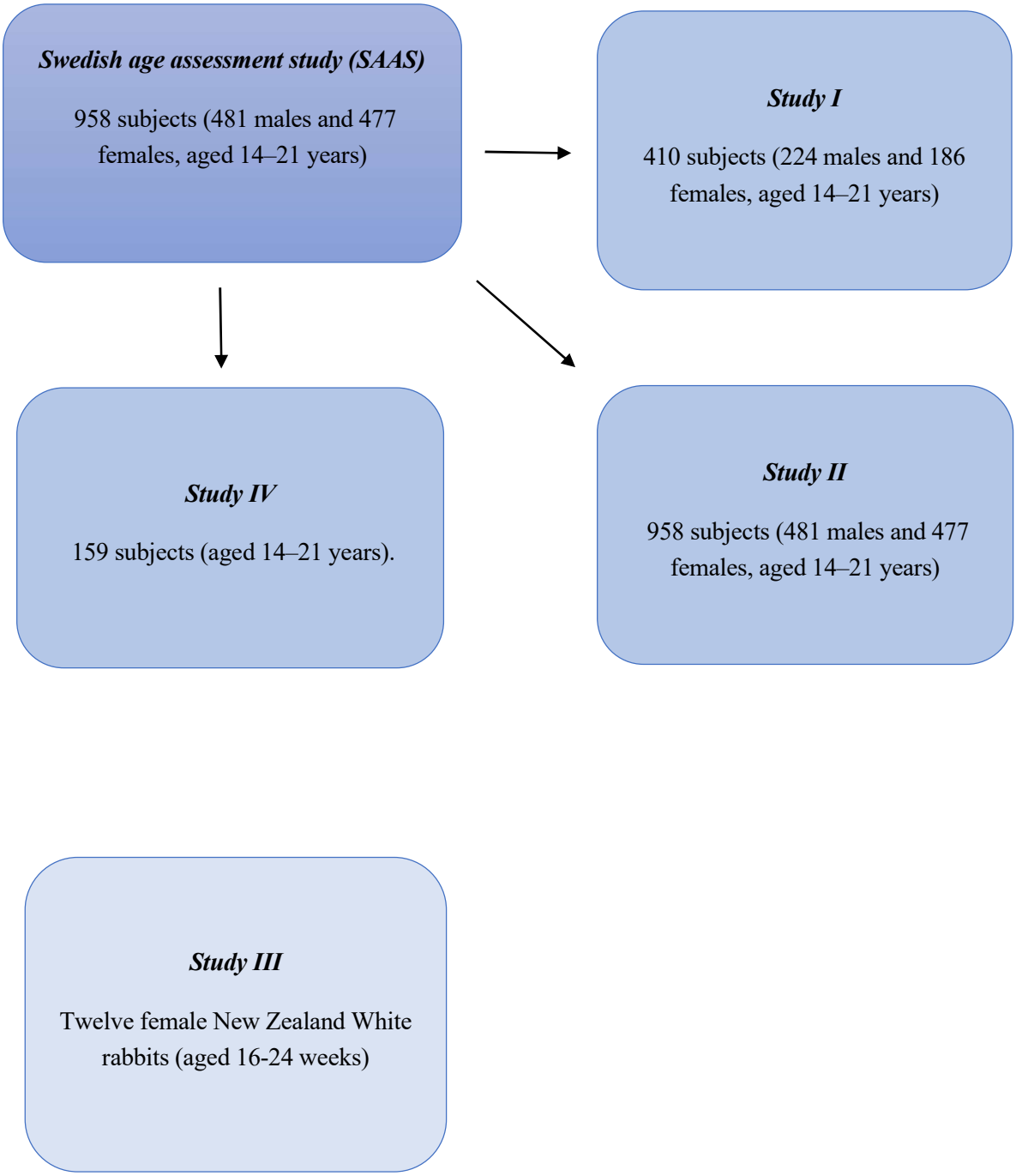

Figure 7. Flowchart of inclusion in the studies.

5.1.1 Human population and ethical considerations

The studies with human study populations, *Study I, II* and *IV*, were prospective, cross-sectional studies of healthy volunteers (subjects). The recruitment was done as part of the Swedish age assessment study (SAAS) and was endorsed by the Swedish National Board of Health (*Socialstyrelsen*). The entire study population consisted of 481 females and 477 males, 958 in total, aged between 14.0-21 years of age. The study was approved by the local ethics committee with the registration number 2017/4 – 31/4 including amendments regarding pregnancy testing (registration number 2017/1184-32) and DTI (registration number 2017/1773-32). All studies were performed in accordance with the Declaration of Helsinki between 2017 and 2018.

All participants, from now on called subjects, and legal guardians of minors, received written information about the SAAS study when they were asked to participate. The information letter had a different readability score depending on the intended reader. The information letter to minors had a readability index (LIX) of 35. An index of 35 represents the educational level of junior high school (grade 6 – 9) and the same degree of difficulty as easy-to-read fiction [165]. Therefore, every subject should have been able to comprehend the information. Participation was voluntary and written consent was acquired from all subjects, including legal guardians of minors.

The inclusion criteria were:

1) healthy individual without prior illness that may have affected the growth plate directly or indirectly (for example long term cortisone medication)
2) born in Sweden (verified by birth certificate).

The exclusion criteria were:

1) having lived outside Sweden for a period longer than six months
2) history of bilateral trauma near the growth plate
3) chronic disease or long-term medical treatment that might affect growth velocity i.e., the growth plate
4) pregnancy
5) non-compliance during the exam.

Female subjects took pregnancy tests prior to the MRI examination to ensure that no subject was pregnant at the time of examination.

The clavicle was not included in *Study II* because it is a moving object, and therefore difficult to image with MRI, and due to the various anatomical variations of the growth plate [96].

Examination of this anatomical site would have required a long time of acquisition with unknown quality and was therefore excluded to the benefit of the other chosen locations. Data were coded in accordance with routine and are stored in locked firesafe facilities.

5.1.2 Animal population and ethical considerations

The animal experiment (*Study III*) was performed in accordance with Swedish National Board of Laboratory guidelines and was approved by the regional laboratory animal ethics committee according to the *Animal Welfare Act* (*Ch. 7 § 9. Animal Welfare Act SFS 2018: 1192*) with registration number 14436-2019. Animal experiments must show a benefit for the greater good and the avoidance of unnecessary suffering.

Twelve female New Zealand white rabbits (NZW) (16-, 20- or 24 weeks old, four in each age group) were selected to simulate adolescence in girls [130]. The rabbits were premedicated with a subcutaneous injection of Medetomidine 0,5 mg/kg and then euthanized by an overdose of pentobarbital injection administrated through the lateral auricular vein. Euthanization prior imaging was a measure to reduce the suffering for the NZW. The hindlimbs were separated from the body prior to imaging to improve image quality. The hindlimbs were imaged immediately after euthanization. The knee joints were arranged and fixed in an extended position side-by-side (Figure 8). The hindlimbs were then positioned in a prone position before imaging.

Figure 8. Euthanized rabbit after fatal pentobarbital injection through the lateral auricular vein (left image). The separated hindlimbs in a supine position with visible patella and patellar tendon (middle image). The separated hindlimbs were fixed in a prone position in the coil using tape and a condom (right image).

After imaging the soft tissues were removed from the bones before the hindlimbs were separated for histology and μCT. The right hindlimbs were used for histology. Both femur and tibia were cut in the frontal plane with a bone saw. The samples were then fixed in 4% paraformaldehyde solution and stored in room temperature for 48 hours, followed by decalcification in buffered 15% EDTA solution for 4 to 6 weeks at 4 °C (Figure 9). The left hindlimb was used for μCT and was fixed in 70 % ethanol solution and kept in cold storage until scanning.

Figure 9. After imaging the soft tissues are removed around the femur (left image). The femur is then fixed in 70 % ethanol (right image)

5.2 IMAGE PROTOCOLS

5.2.1 MRI

5.2.1.1 Study I and II

The non-dominant side was imaged except for in subjects who reported injury near the growth plate, in which case the dominant side was pictured instead.

Study I focused on the knee joint and used cartilage-dedicated and T1W images. *Study II* used only cartilage-dedicated sequence images and imaged five different anatomical locations (calcaneus, proximal and distal tibia, distal femur, and the radius). All subjects were examined with 1.5 T whole-body MRI scanners from three vendors (General Electric, Siemens, and Philips) at three different locations.

The chosen image planes varied by anatomical site. The wrist was imaged in the coronal plane. The knee was imaged in the coronal plane on cartilage-dedicated sequence and the sagittal plane with the T1W used in *Study I*. The ankle was imaged in the sagittal plane.

Protocols varied slightly by scanner manufacturer and anatomical site.

T1W:
All T1W sequences are routinely used in clinical practice. Technical specifications were the following:

General Electric: 2D fast-spin echo (FSE), TE/TR= 7.6/406 ms, flip angle 90°, slice thickness 3 mm with 4 mm spacing.

Philips: 2D turbo-spin echo (TSE), TE/TR= 17/458 ms, flip angle 90°; slice thickness 3 mm with 3.3 mm spacing.

Siemens: 2D TSE, TE/TR= 12/600 ms, flip angle 90°, slice thickness 3 mm with 3.3 mm spacing.

Common settings: Field of view (FOV)= 160 x 160 mm, matrix= 256 x 256, resolution= 0.625 x 0.625 mm. The images were acquired in sagittal orientation and time of acquisition was approximately 4 – 5 min.

Cartilage dedicated sequence:

General Electric: 3D-MERGE gradient echo (GRE) with fat saturation, TE/TR= 18/40 ms, and flip angle 15°.

Philips: 3dWATSc-GRE with fat saturation, TE/TR= 7.61/20 ms, and flip angle 25°.

Siemens: MEDIC-3D-GRE with fat saturation, TE/TR 14/45 ms, and flip angle 12˚.

Common settings for each joint were the following:

Wrist: FOV= 120 x 120 mm, matrix= 208 x 208, resolution= 0.58 x 0.58 mm, slice thickness of 2 mm with 2 mm spacing.

Knee: FOV= 160 x 160 mm, matrix= 272 x 218, resolution= 0.58 x 0.73 mm, slice thickness of 3 mm with 3 mm spacing, a pixel.

Ankle: FOV= 150 x 150mm, matrix 300 x 161, resolution= 0.5 x 0.93 mm, slice thickness of 3 mm with 3 mm spacing.

Each sequence was about 4-5 min and the total examination time for all anatomical locations was less than 30 min.

5.2.1.2 Study III

MRI examinations were performed using a 9.4 Tesla preclinical MRI scanner (Varian MRI system, Agilent Technologies, Palo Alto, CA, USA). A multi-gradient echo 3D sequence was used to visualize the growth plate cartilage, acquired with the following parameters: FOV= 60 × 60 x 60 mm, matrix= 256 × 256 × 256, resolution= 234 μm isovolumetric voxel size, TR= 30 ms, and flip angle of 30°. The following echo times (TE) were used: 1.46, 3.74, 6.22, and 8.60 ms with 16 dummy scans. The total acquisition time for the multigradient echo 3D sequence was 30 min and 4 s.

5.2.1.3 Study IV

The MRI images used to evaluate the growth plate of the knee are the same as described in *5.3.1.1* under the section “cartilage dedicated sequence”.

5.2.2 DTI

5.2.2.1 Study III

A diffusion-weighted spin-echo sequence was used for the DTI with the following technical specifications: 28 slices, no gap, and slice thickness of 1 mm. FOV= 90 × 60 mm^2, matrix= 256 × 128, resolution= 350 × 460 μm, TE/TR= 25.6/2500 ms. The readout gradient was parallel to the magnetic field and the phase-encode direction from left to right with four dummy scans.

The diffusion encoding and decoding gradients were 4 ms long with an amplitude of 15.93 mT/m separated by 16 ms resulting in a b-value of 984 s/mm^2. DTI images were acquired along 14 diffusion directions in addition to 2 reference images. The total acquisition time for the DTI sequence was 1 h, 15 min, and 50 s.

5.2.2.2 Study IV

The non-dominant knee was examined with an echo-planar DTI on a 3.0T Philips Ingenia MR whole-body scanner (Philips Medical System, Best, Netherlands). Sagittal images with a fat-saturation were acquired with the following parameters: FOV=150 x 150 x 82 mm, resolution= 2 x 2 x 3 mm, TE/TR= 80/7100 ms. Diffusion was done in 15 directions, with a b- value of 0 and 600s/mm^2. The corresponding acquisition time was 04:40min.

5.2.3 Histology

High-resolution images of the growth plate were obtained with a panoramic digital slide scanner (3DHISTECH Ltd, Budapest, Hungary) and height measurements were made with CaseViewer software (3DHISTECH).

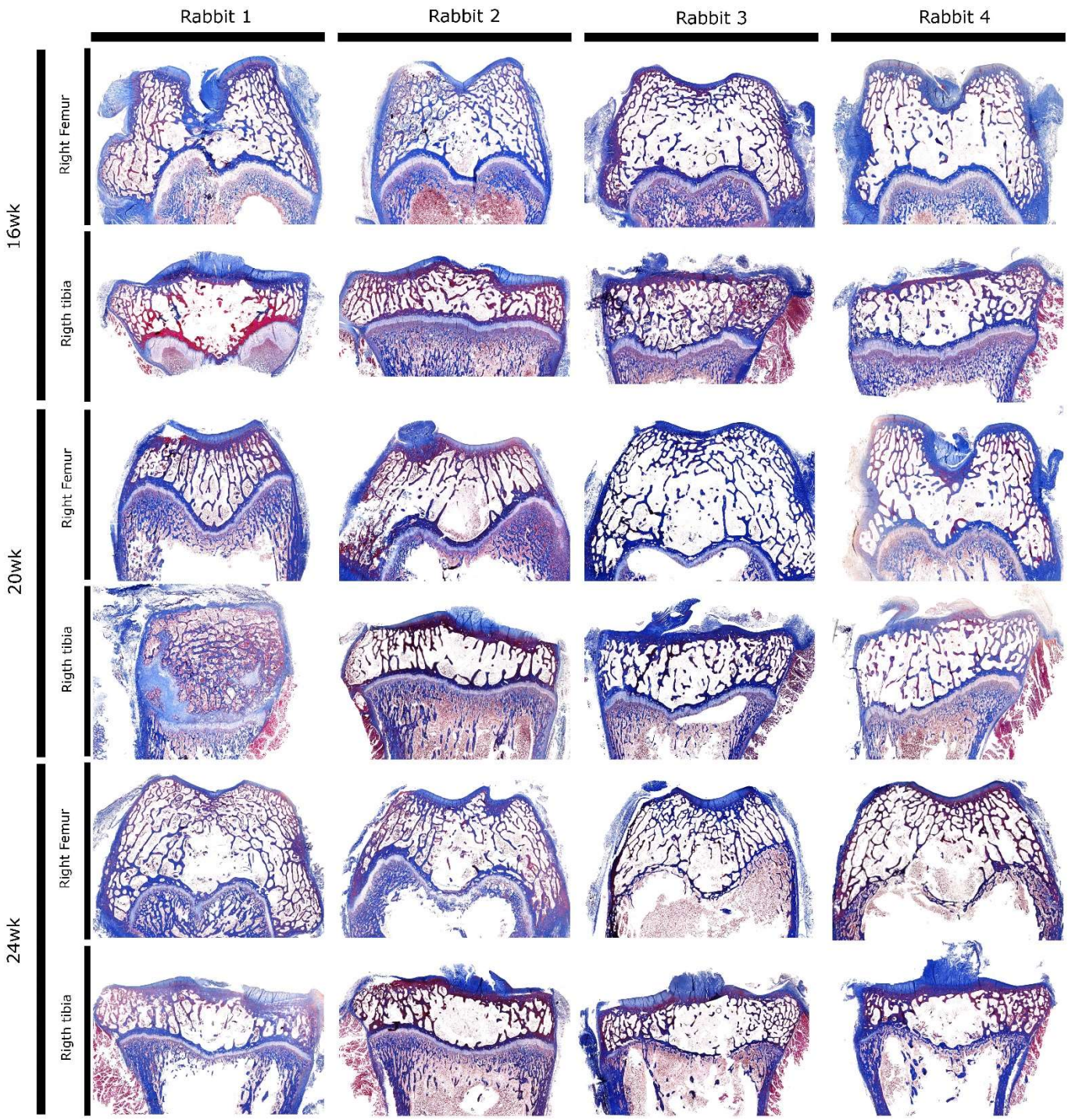

Figure 10. A summary of histological samples (Masson's trichrome staining) from the rabbits in *Study III*. Each column represents a rabbit and each row an anatomical location (distal femur or proximal tibia) as well as age of rabbit. Wk= weeks old. (Reprinted with permission from Z. Dou)

5.2.4 µCT

An X-ray microscope (XRM) and Zeiss Xradia Versa 520 lab-based scanner (Carl Zeiss X-ray Microscopy, Pleasanton, CA, USA) was used to acquire the µCT images. The image settings were emission source set at 80 kV and 7 W with an LE4 source filter. A 0.4× objective was used, and the samples were placed 3.8 mm from the source and 8.9 mm from the detector. This resulted in a FOV= 20.9 × 20.9 mm, matrix= 1024 × 1024 pixels, resolution= 20 µm isovolumetric voxel size. An exposure time of 2 s and step size of 0.45° resulted in a total of 801 images and acquisition time of 40 min and 32 s.

5.3 IMAGE ANALYSIS

5.3.1 Study I and II

Individuals were anonymized at the time of imaging, so the only DICOM information available was the individual participant number and the technical DICOM information from the whole-body MRI scanner.

Images were evaluated on a local picture archiving and communication system (PACS). The image with the most mature growth plate closure was selected and graded. The images with the highest grade of closure were rated according to a staging system created from previous studies [49, 55, 79]. The modified scale was the following:

Stage 1. A continuous and stripe-like growth plate with cartilage signal intensity is present between the metaphysis and the epiphysis. The growth plate has a thickness greater than 1.5mm and multilaminar appearance.
Stage 2. A continuous growth plate with cartilage signal intensity is present between the metaphysis and the epiphysis. The growth plate has a thickness greater than 1.5mm but does not have multilaminar appearance.
Stage 3. A continuous growth plate with cartilage signal intensity is present between the metaphysis and the epiphysis. The growth plate thickness is less than 1.5mm.
Stage 4a. The growth plate cartilage is not continuous. An epiphyseal-metaphyseal fusion is represented by a hazy area involving one third or less of the growth plate.
Stage 4b. The growth plate cartilage is not continuous. An epiphyseal-metaphyseal fusion is represented by a hazy area involving between one third and two thirds of the growth plate.
Stage 4c. The growth plate cartilage is not continuous. An epiphyseal-metaphyseal fusion is represented by a hazy area involving more than two thirds of the growth plate.
Stage 5. The growth plate is completely fused on all images, with or without an epiphyseal scar. (Figure 11)

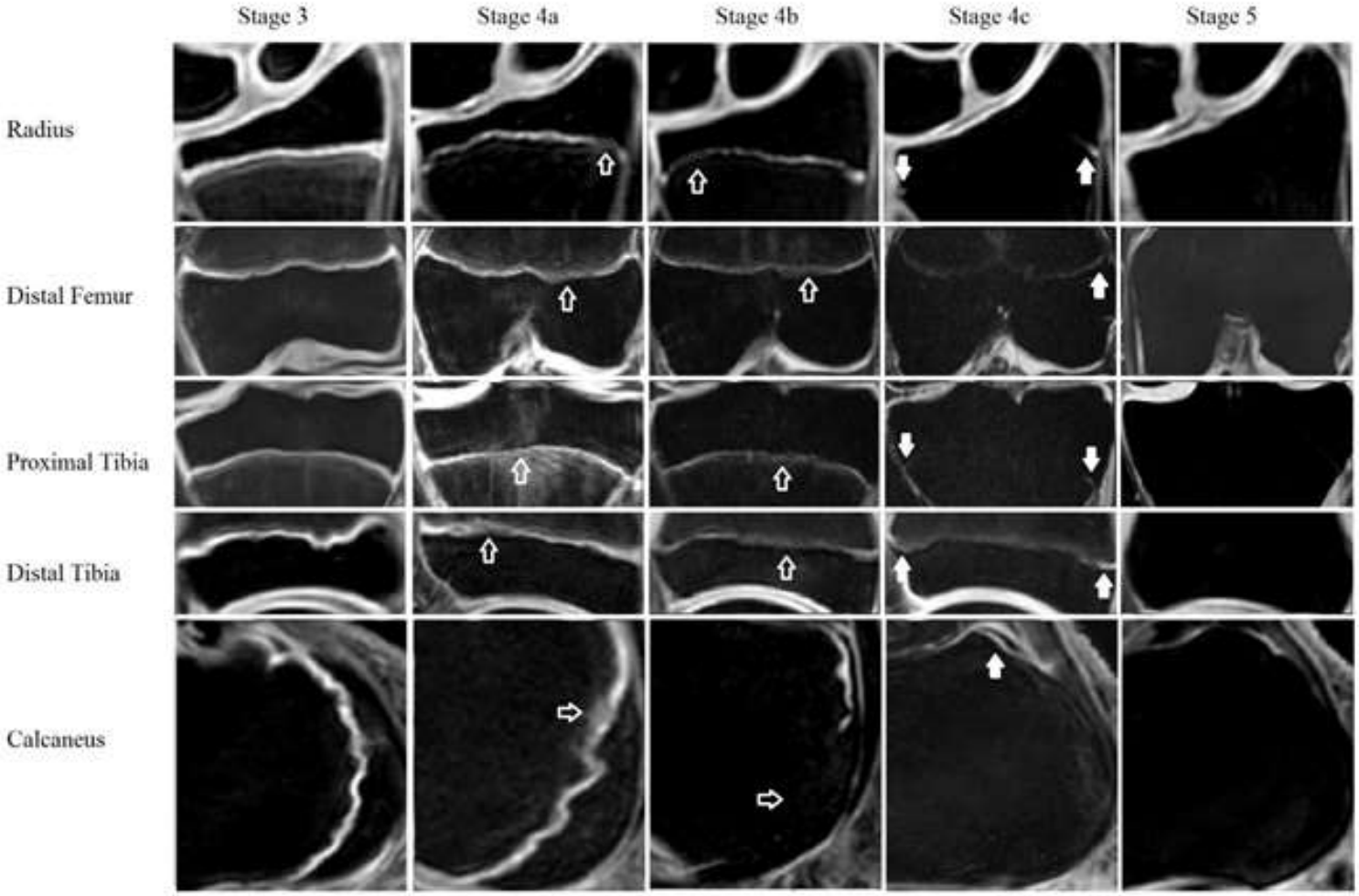

Figure 11. Image from *Study II.* Each column represents a stage of closure and each row an anatomical location. Open white arrows indicate areas of bone bridging in stage 4a and 4b. The solid white arrows indicate unfused growth plate in stage 4c. (Reprinted with permission from Wiley)

5.3.2 Study III

5.3.2.1 MRI

The growth plates were manually traced on the multi-gradient echo 3D sequence using the ITK Snap ITK Snap software version 3.8.0 (http://itksnap.org). The volume of the growth plate was then calculated. The central part of the growth plate was selected in coronal plane, then sectioned into ten portions. The height measurements were taken and averaged.

DSI Studios was used (http://dsi-studio.labsolver.org) for the DTI measurements. Each region was manually traced by two different radiologists. From the traced regions DTI metrics were measured and tractography was performed. A minimum FA value threshold of 0.04 and maximum turning angle of 45° was used based on previous animal studies [137, 138]. All tracts from the tractography (number of tracts, tract length and volume) were included and used in the statistical analysis.

5.3.2.2 µCT

Object Research Systems Dragonfly (Montreal, Canada) was used to identify the non-mineralized growth plate, define it as a region of interest, and calculate its volume (Figure 12).

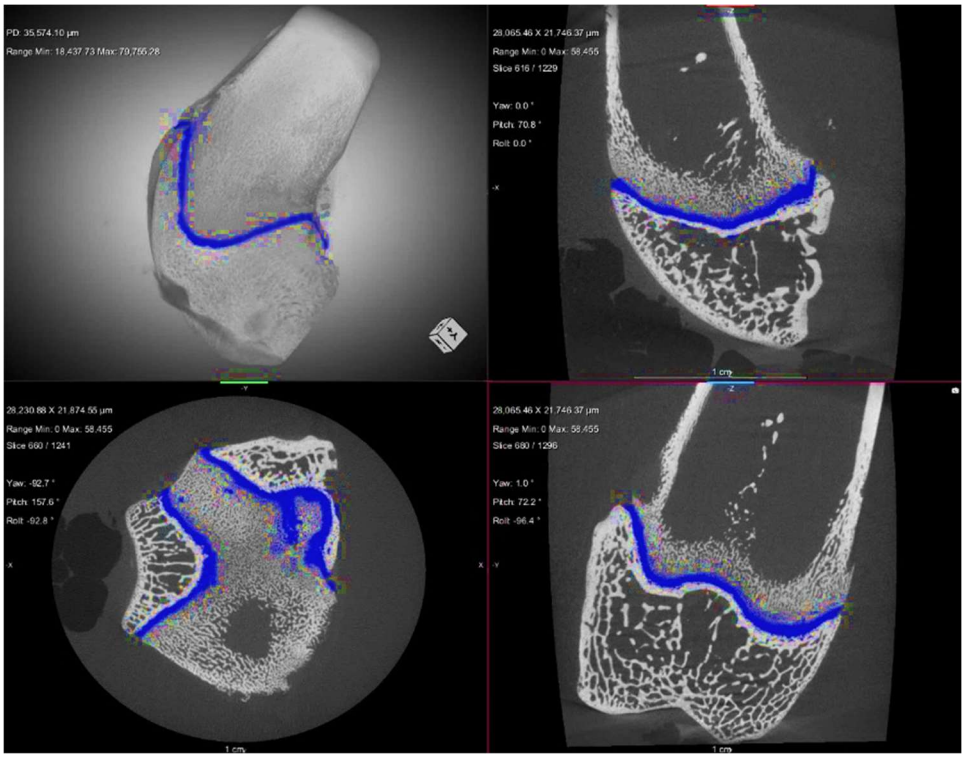

Figure 12. The growth plate has been traced on µCT with isovolumetric voxels. (The tracing is indicated in blue. The upper left image is a 3D view and the others represent sagittal (upper right), axial (bottom left) and coronal (bottom right) views of a femur in a 16-week-old rabbit. (Image is obtained from the Dragonfly software)

A coronal section was selected in the central part of the growth plate, and the growth plate was divided into ten separate sections. In each section the height of the growth plate was measured (Figure 13). The ten individual measurements were averaged for the statistical analysis.

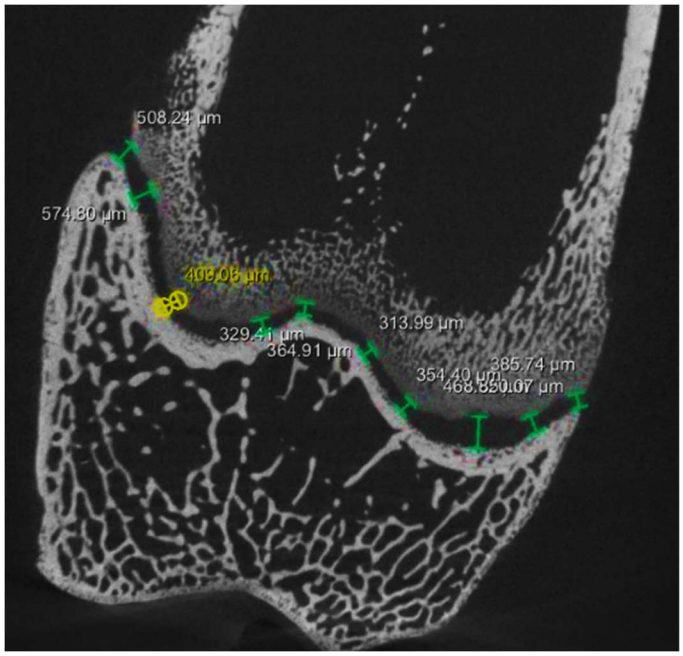

Figure 13. Detailed image of height measurements in coronal view on µCT images. (Image is obtained from the Dragonfly software)

5.3.2.3 Histology

The height measurements were done with the CaseViewer software by measuring the from the border between the secondary ossification center and the growth plate cartilage to the border between the growth plate cartilage and the metaphysis. A coronal section was selected in the central part of the growth plate, and measurements were performed parallel to the chondrocyte columns i.e., perpendicular to the growth plate borderlines. The ten individual measurements were averaged for the statistical analysis.

5.3.3 Study IV

The cartilage-dedicated assessments of the growth plate closure of the subjects completed in *Study II* were used in *Study IV*.

The DTI assessment was performed on DSI Studio (http://dsi-studio.labsolver.org). The growth plate was traced manually on *b0* sagittal images to create a volume of interest. In case

of a closed growth plate, the physeal scar was traced if it was detectable on *b0* images. After a six-month washout period, all images were re-traced by the same paediatric radiologist to calculate intra-observer agreement. From the traced regions DTI metrics were measured and tractography was performed. The minimum FA value threshold of 0.04 and maximum turning angle of 45° were chosen based on previous studies [121, 122]. All tracts from the tractography (number of tracts, tract length and volume) were included and used in the statistical analysis.

5.4 STATISTICS

Study I: The inter- and intra-observer agreement was measured in Kappa (κ) and the inter- and intra-reliability was measured by intraclass correlation coefficient (ICC).

The Kappa values were interpreted as follows: <0.2 poor agreement; 0.2-0.4 fair agreement; 0.4-0.6 moderate agreement; 0.6-0.8 good agreement; 0.8-1.0 very good agreement [166].

The ICC values were interpreted as follows: <0.5 poor agreement; 0.5-0.75 moderate agreement; 0.75-0.9 good agreement; 0.9-1.0 excellent agreement [167].

SPSS version 25.0 for Windows (IBM Corp., Armonk, NY, USA) was used for the statistical analyses.

Study II: Weighted Kappa (κ) was calculated to evaluate the inter- and intra-observer agreement. Spearman's ranks correlation coefficient was used to evaluate the correlation between the chosen factors. The Spearman's rank correlation (ρ) were interpreted as the following: 0 – 0.1 (or 0 – -0.3) negligible correlation; 0.1 – 0.39 (or 0 – -0.39) weak correlation; 0.4 – 0.69 (or -0.4 – -0.69) moderate correlation; 0.7 – 0.89 (-0.7 – -0.89) strong correlation; 0.9 – 1 (-0.9 – -1.0) very strong correlation [168].

Logistic regression was performed to evaluate at what age the growth plate was completely fused (stage 5). Multiple logistic regressions were performed to calculate the odds ratio for each growth plate. Stage 5 was used as a dependent variable, whereas age, sex and BMI were used as independent variables. A further evaluation of whether BMI affected the growth plate maturity was performed by conditional logistic regression stratified for age and sex.

R software package, version 3.5.3, (The R Project for Statistical Computing) was used for the statistical analysis. A P-value of <0.05 was considered significant. All calculations were done by a statistician at the Department of Learning, Informatics, Management and Ethics (LIME), Karolinska Institute.

Study III: Wilcoxon signed rank test was used to compare MRI, histomorphometry, and μCT. ICC were used to measure inter-observer agreement. Correlation between measures were assessed with Pearson's. The Pearson's correlation coefficient (*R*) values were interpreted as the following: 0 – 0.1 (or 0 – -0.3) negligible correlation; 0.1 – 0.39 (or 0 – -0.39) weak correlation; 0.4 – 0.69 (or -0.4 – -0.69) moderate correlation; 0.7 – 0.89 (-0.7 – -0.89) strong correlation; 0.9 – 1 (-0.9 – -1.0) very strong correlation [168].

SPSS Statistics v. 28.0 (IBM, Armonk, NY, USA) was used for the statistical analyses. A *P*-value < 0.05 was considered significant.

Study IV: Wilcoxon signed-rank tests were performed to compare the DTI metrics and tractography between the femoral and tibial growth plate. ICC was used to measure intra-observer agreement. Correlation between measures was assessed with Pearson's.

SPSS Statistics v. 28.0 (IBM, Armonk, NY, USA) was used for the statistical analyses. A *P*-value < 0.05 was considered significant.

6 RESULTS

6.1 STUDY I

The ICC was overall excellent. There was a performance difference between pediatric and general radiologists (Table 1).

T1W: The inter- observer agreement was higher for pediatric radiologists (femur: κ= 0.73; tibia: κ = 0.82) compared to general radiologists (femur: κ = 0.56; tibia: κ= 0.34).

The intra-observer agreement was (κ= 0.65) for the femur and (κ= 0.75) for the tibia.

Cartilage-dedicated sequence: There was a higher inter- and intra-observer agreement compared to T1W with inter-observer agreement of (κ= 0.86) for the femur and (κ= 0.90) for the tibia.

The intra-observer agreement was (κ= 0.79) for the femur and (κ= 0.81) for the tibia.

	Femur				Tibia			
	T1W-TSE		Cartilage sequences		T1W-TSE		Cartilage sequences	
	Kappa	ICC	Kappa	ICC	Kappa	ICC	Kappa	ICC
Inter- observer agreement pediatric radiologists	0.73 (82%)	0.96 (0.94 – 0.98)	0.86 (93%)	0.96 (0.95 – 0.97)	0.82 (90%)	0.97 (0.96 – 0.98)	0.90 (95%)	0.96 (0.95 – 0.97)
general radiologists	0.56 (69%)	0.95 (0.94 – 0.96)			0.34 (56%)	0.90 (0.87 – 0.93)		
Intra- observer agreement pediatric radiologist	0.65 (77%)	0.95 (0.93 – 0.96)	0.79 (89%)	0.96 (0.95 – 0.97)	0.75 (87%)	0.95 (0.94 – 0.96)	0.81 (91%)	0.96 (0.95 – 0.97)

Table 1. Summary of the observer agreement in Kappa (κ), percentage agreement in parentheses, and intra-class correlation coefficients (ICC) including 95% confidence intervals in parentheses. (Reprinted with permission from SAGE journals)

ICC= Intraclass correlation coefficient; 95% CI= 95% confidence interval; TSE= Turbo Spin Echo Sequence

6.2 STUDY II

Growth plate closure occurred in ascending direction from the calcaneus to the radius (Table 2). Ages when growth plate closure was seen in all individuals are indicated in bold. Complete fusion seems to occur approximately 2 years earlier in girls than in boys.

Gender	Age	Radius	Femur	Proximal Tibia	Distal Tibia	Calcaneus
Male	14	0/59 (0%)	0/60 (0%)	0/60 (0%)	3/60 (5.0%)	11/60 (18.3%)
	15	1/59 (1,7%)	0/60 (0%)	2/60 (3.3%)	11/60 (18.3%)	31/59 (52.5%)
	16	5/60 (8.5%)	10/60 (16.7%)	12/60 (20.0%)	35/60 (58.3%)	46/60 (76.7%)
	17	15/61 (24.6%)	26/61 (42.6%)	34/61 (55.7%)	54/61 (88.5%)	60/61 (98.4%)
	18	34/57 (59.6%)	48/58 (82.7%)	50/57 (87.7%)	57/58 (98.3%)	**58/58 (100%)**
	19	52/58 (89.7%)	58/60 (96.7%)	57/60 (95.0%)	58/60 (96.7%)	59/60 (98.3%)
	20	53/54 (98.1%)	**54/54 (100%)**	**54/54 (100%)**	52/54 (96.3%)	**54/54 (100%)**
	21	**59/59 (100%)**	**60/60 (100%)**	**60/60 (100%)**	**60/60 (100%)**	**60/60 (100%)**
Female	14	3/62 (4.8%)	6/62 (9.7%)	12/62 (19.4%)	31/62 (50%)	44/61 (72.1%)
	15	8/60 (13.3%)	25/62 (40.3%)	33/62 (53.2%)	52/62 (83.9%)	56/62 (90.3%)
	16	26/60 (43.3%)	42/60 (70.0%)	53/60 (88.3%)	55/59 (93.2%)	56/58 (96.6%)
	17	45/60 (75.0%)	51/60 (85.0%)	58/60 (96.7%)	59/60 (98.3%)	59/60 (98.3%)
	18	55/61 (90.2%)	59/60 (98.3%)	**60/60 (100%)**	**61/61 (100%)**	**61/61 (100%)**
	19	**57/57 (100%)**	**58/58 (100%)**	**58/58 (100%)**	**58/58 (100%)**	**58/58 (100%)**
	20	**57/57 (100%)**	**57/57 (100%)**	**57/57 (100%)**	**57/57 (100%)**	**57/57 (100%)**
	21	**60/60 (100%)**	**60/60 (100%)**	**60/60 (100%)**	**60/60 (100%)**	**60/60 (100%)**

Table 2. Number of subjects with a completely closed growth plate (Stage 5) at each anatomical location. The values presented as a ratio and percentage for females and males in each age group. (Reprinted with permission from Wiley.)

Spearman's rank correlation coefficient was calculated separately for each sex. There was a weak to moderate correlation (ρ= 0.287 – 0.513; *P*< 0.001) between sexual maturation (Tanner) and growth plate maturity at the various anatomical sites in females. The correlation was moderate (ρ= 0.514 – 0.598; *P*< 0.001) between the same variables in males.

BMI showed a weak correlation with growth plate maturation in both females (ρ= 0.186 – 0.222; *P*< 0.001) and males (ρ= 0.308 – 0.384; *P*< 0.001). The only significant correlation seen between physical activity and growth plate maturation was in the female radius, but the correlation was negligible (ρ= 0.095; *P*< 0.05).

The multiple logistic regression model showed an odds ratio of 8.57 – 28.81 (*P*< 0.01) that females were more likely to be stage 5 than males, depending on the anatomical site. An individual is more likely, at odds ratio: 4.18 – 5.62, to have a fully mature growth plate for each additional year of age depending on the anatomical site. Conditional logistic regression demonstrated that being overweight increased the likelihood of being stage 5 by an odds ratio: 2.65 – 8.71; *P*< 0.05, in all the anatomical locations for females except the proximal tibia. Males only had increased odds ratios in the radius (odds ratio 4.03; *P*< 0.01) and distal tibia (odds ratio 2.97; *P*< 0.05) (Table 3).

	Radius	Femur	Proximal Tibia	Distal Tibia	Calcaneus
Male	**4.03** ***P*< 0.01**	2.45 *P*< 0.1 (*P*= 0.087)	2.50 *P*< 0.1 (*P*= 0.073)	**2.97** ***P*< 0.05** **(*P*= 0.026)**	1.71 *P*< 0.3 (*P*= 0.258)
Female	**2.65** ***P*< 0.01**	**2.73** ***P*< 0.01**	3.02 *P*= 0.11	**4.23** ***P*< 0.02**	**8.71** ***P*< 0.05**

Table 3. Conditional logistic regression stratified for age and gender to calculate odds ratio for overweight individuals to be stage 5 in comparison to their peers. The significant findings are indicated in bold letters. (Reprinted with permission from Wiley.)

6.3 STUDY III

6.3.1 Morphometry

Both height and volume of the distal femur and proximal tibial growth plates declined with age in all modalities and the maturation process can be visualized macroscopically in both the distal femur and proximal tibia (Figure 14). Wilcoxon signed-rank test did not show a difference between the height and volumetric measurements.

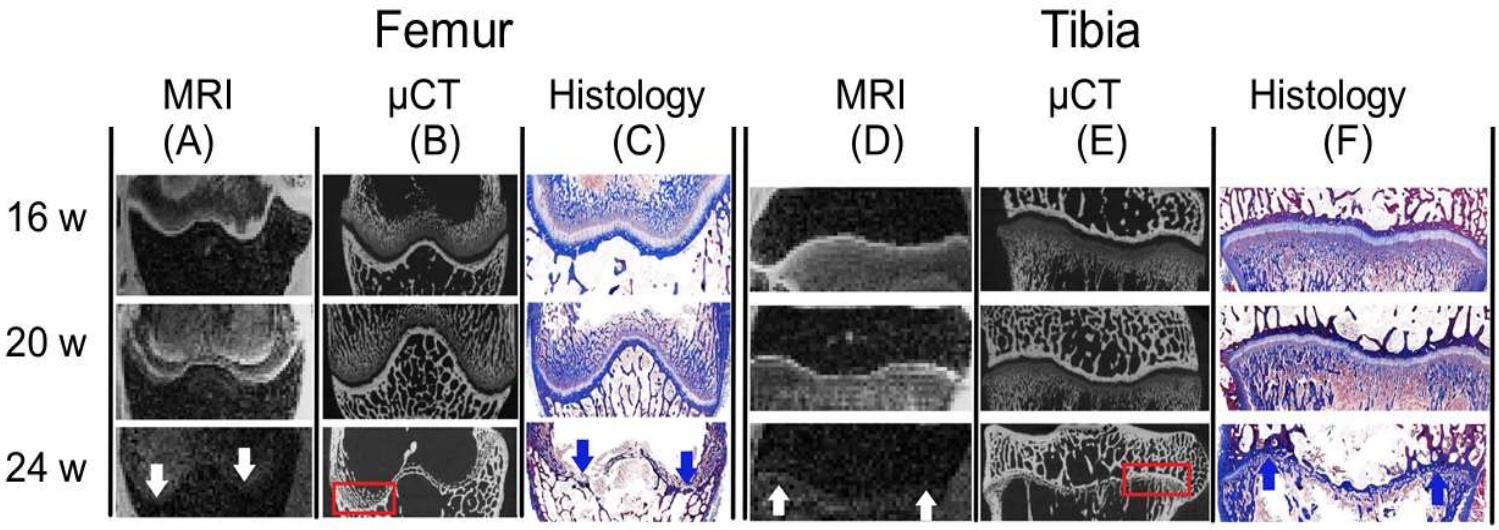

Figure 14. Coronal cross-section of the growth plate on MRI (multi-gradient echo 3D sequence), µCT, and histology (Masson's trichrome staining). Each column represents a modality and anatomical location while each row represents an age group.

MRI: The growth plate (A= femur; D= tibia) has a high signal on MRI in the 16-week-old rabbit. The growth plate is not visible (white arrows) in the 24-week-old NZW.

µCT: The growth plate has a low attenuation in anatomical locations (femur= B; tibia= E). Early bone bridging can be seen in the 20-week-old NZW while it the growth plate appears fused (red boxes) in the 24-week-old NZW.

Masson's trichrome staining: The growth plate appears as light blue colored in 16- and 20-week-old NZW in both anatomical locations (C= femur; F= tibia). The fused growth plate appears as a dark blue sclerotic rim in the 24-week-old NZW. This finding has been referred to as a physeal scar (blue arrows).

Two out of four 24-week-old rabbits had a completely fused growth plate. (Reprinted with permission from Wiley.)

6.3.2 DTI

The colored FA map shows horizontal diffusion in the central portion (proliferative zone) of the growth plate, and diffusion perpendicular to the growth plate in the transitional zone between the growth plate and the metaphysis. High-resolution images of the growth plate on μCT showed a brush-like appearance of the transitional zone where the hypertrophic zone transitions to the metaphysis (Figure 15).

Figure 15. Image of the proximal tibia in a 16-week-old NZW from *Study III*. The growth plate is visible as a dark band and below it one can see the brush-like appearance of the hypertrophic zone in transition to the metaphysis on μCT. The mineralized extracellular matrix is visible as white columns in between the hypertrophied chondrocytes (not visible). (Reprinted with permission from Wiley.)

The tract number and volume were highest in the 16-week-old and decreased over time. In contrast, tract length peaked with the greatest observed tract length in the 20-week-old. The FA-value increased with time, inversely proportional to the MD, AD, and RD values which declined with age.

Wilcoxon signed-rank test showed a difference between the tibial and femoral tract length and volume in the 16- and 20-week-old rabbits. 16-week-old rabbits had lower DTI metrics (FA, MD, AD, and RD) in the tibia compared to the femur.

The inter-observer agreement (ICC) was excellent for the femur and good for the tibia with regard to the MD, AD, and RD values at both anatomical sites. The FA value was excellent for the femur and moderate for the tibia. The ICC was moderate regarding the number of tracts at both anatomical locations. There was good inter-observer agreement regarding the tract volume in the femur. However, no significant correlation was seen in the tibia.

Pearson's correlation coefficient (*R*) for the different variables was significant in both the femur and tibia. A negative correlation was observed between age and DTI values (tract length, volume, MD, AD, and RD), except for the FA value, which increased over time at both anatomical sites.

6.4 STUDY IV

FA value had a slight gender difference and increased with age initially before stabilizing MD, RD, tract number and tract volume initially declined with age until they stabilized. (Figure 16 femur, figure 17 tibia)

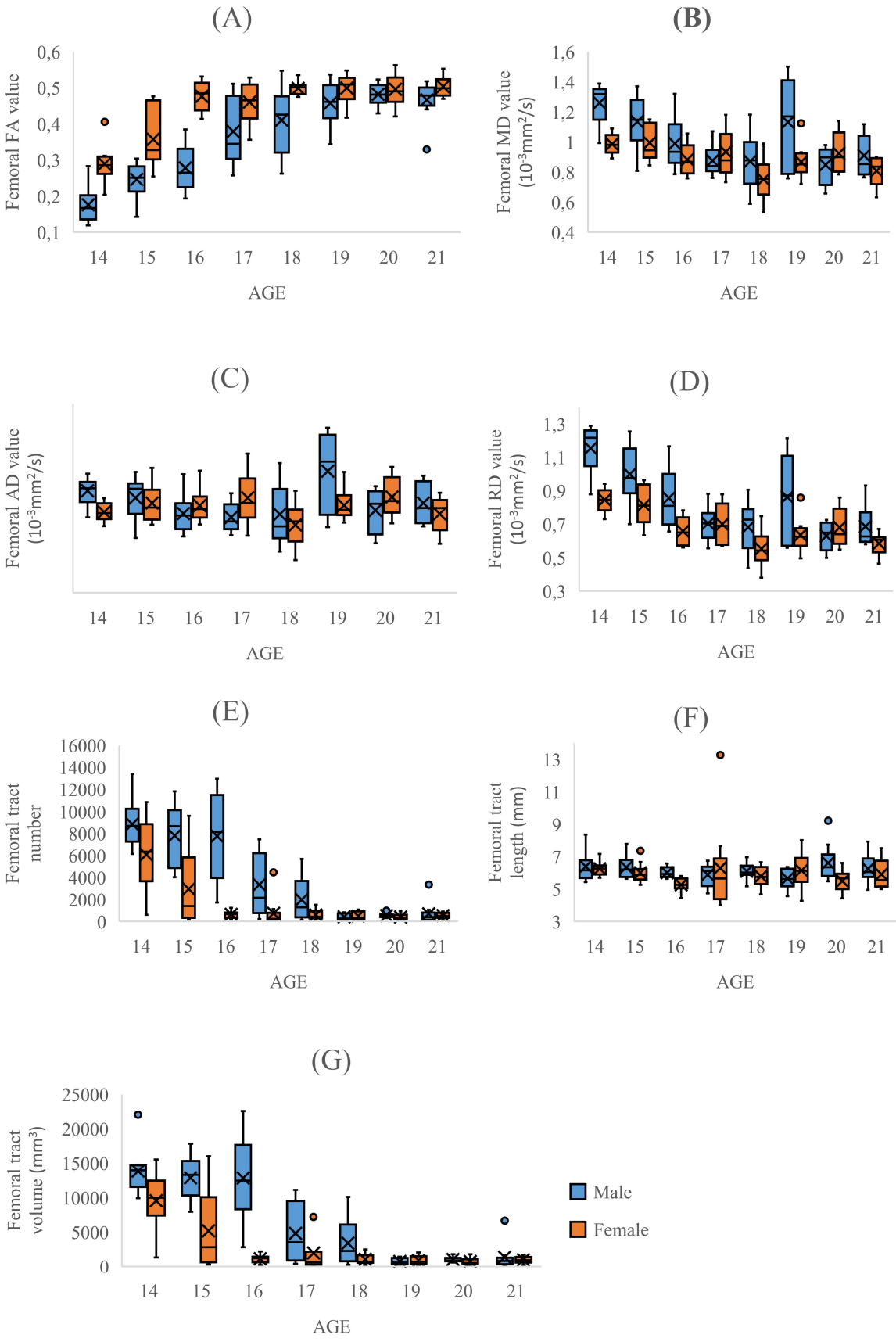

Figure 16. DTI metrics and tractography values of the femoral growth plate organized by the age of the volunteers. The *X* in each boxplot indicates the mean value and the line represents the median value. The orange boxplots are the female values, and the blue boxplots are the male values. A FA; B: MD; C: AD; D: RD; E: tract number; F: tract length; G: tract volume. (FA= fractional anisotropy, MD= mean diffusivity, AD= axonal diffusivity, RD= radial diffusivity.)

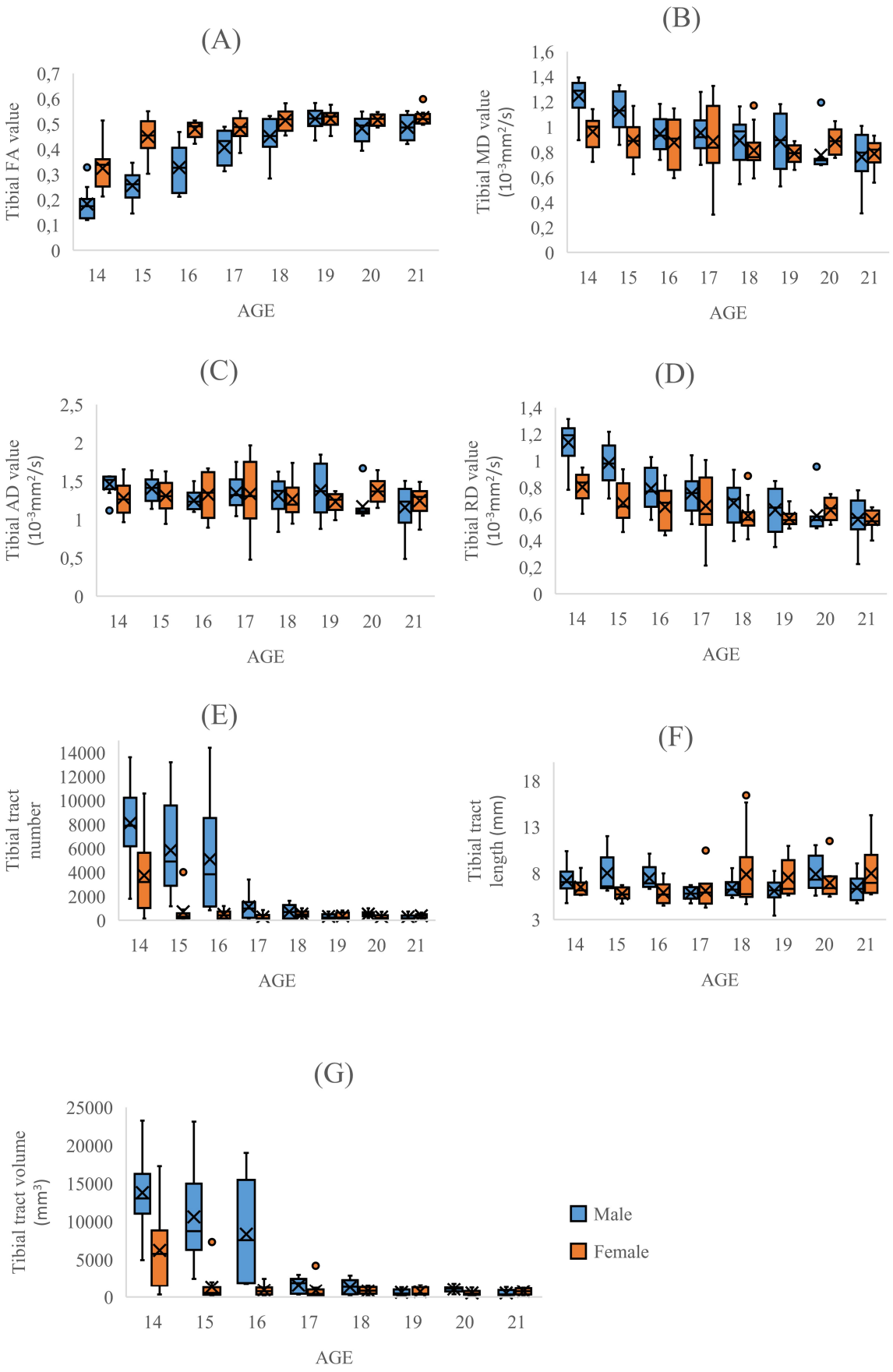

Figure 17. DTI metrics and tractography values of the tibial growth plate organized by age of the volunteers. The *X* in each boxplot indicates the mean value and the line represents the median value. The orange boxplots are the female values, and the blue boxplots are the male values. A FA; B: MD; C: AD; D: RD; E: tract number; F: tract length; G: tract volume. (FA= fractional anisotropy, MD= mean diffusivity, AD= axonal diffusivity, RD= radial diffusivity.)

Wilcoxon signed-rank test indicated a difference between the femoral and tibial tract number ($P< 0.05$) in almost every age group. A difference in tibial and femoral tract volume by age was observed between females (aged 14, 15, 17 and 21) and males (age 16-18 and 21). Similar patterns were seen regarding the difference of the tibial and femoral FA value in 14-15-year-old females compared to 16, 18-19-year-old males.

The intra-observer agreement (ICC) was significant for all the measured variables but varied in how strong the agreement was. The observer agreement regarding the DTI metrics showed an excellent agreement for the FA and RD values on both anatomical sites as well as the MD value in the femoral growth plate. The agreement of the tibial MD values and the AD values on both sites was good. The tractography agreement was excellent regarding tract number at both sites as well as the tibial tract volume, whereas the agreement for the femoral growth plate was only good. Intra-observer agreement for the tract length was moderate on both sites.

Pearson's correlation coefficient *(R)* showed a significant correlation for age as well as for the FA value for all variables at both anatomical sites (femur and tibia). Correlation was negative regarding tractography (tract number and volume), MD and RD values, but positive for the FA value.

The correlation based on skeletal maturation showed slightly different results. The FA was stable in stage 4a and 4b and then increased stepwise. The reverse seen in the MD and RD values: they were stable during 4a and 4b and then declined. Tractography showed an increase of tract number and volume between stage 4a and stage 4b and then a decline in stage 4c and stage 5 for both sexes and anatomical locations. (Figure 18 femur, figure 19 tibia)

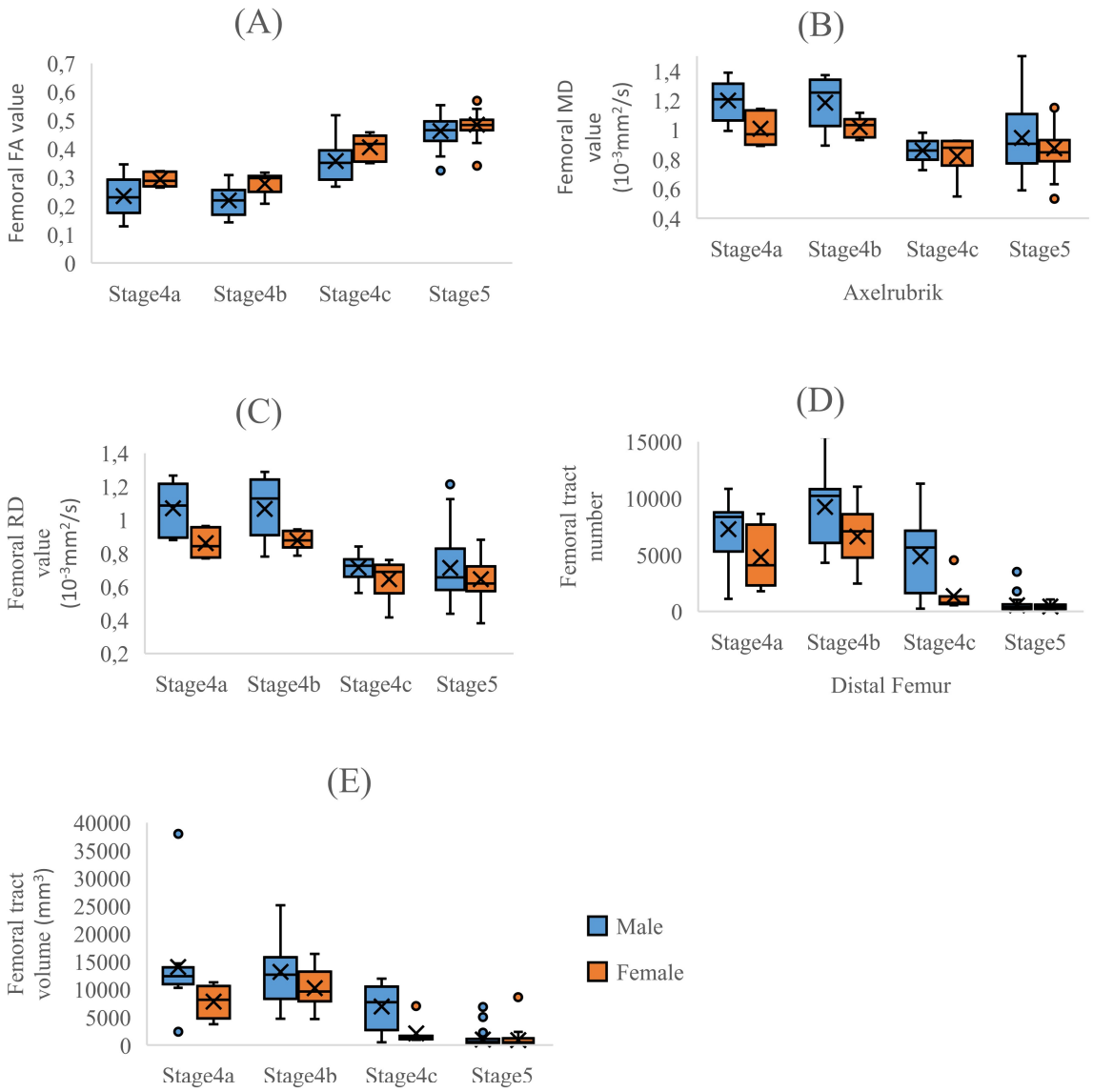

Figure 18. DTI metrics and tractography values of the femoral growth plate organized by the skeletal maturation of the growth plate. The *X* in each boxplot indicates the mean value and the line represents the median value. The orange boxplots are the female values, and the blue boxplots are the male values. A FA; B: MD; C: RD; D: tract number; E: tract volume. (FA= fractional anisotropy, MD= mean diffusivity, RD= radial diffusivity.)

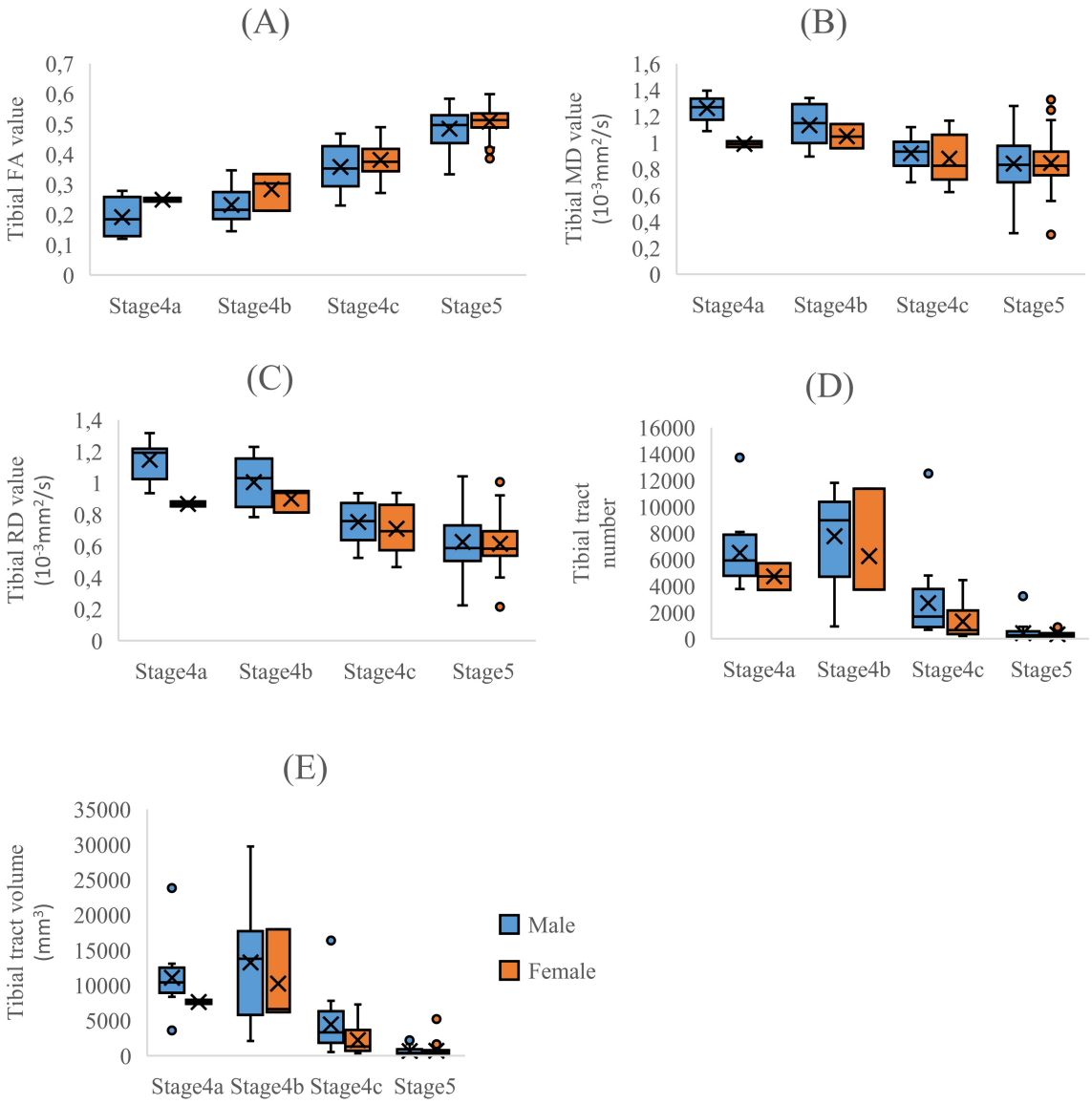

Figure 19. DTI metrics and tractography values of the tibial growth plate organized by the skeletal maturation of the growth plate. The *X* in each boxplot indicates the mean value and the line represents the median value. The orange boxplots are the female values, and the blue boxplots are the male values. A FA; B: MD; C: RD; D: tract number; E: tract volume. (FA= fractional anisotropy, MD= mean diffusivity, RD= radial diffusivity.)

7 DISCUSSION

7.1 GENERAL CONSIDERATIONS REGARDING STUDY DESIGN

It is fundamental that the study population should represent the population we aimed to characterize. The inclusion and exclusion criteria were selected to reduce confounding factors in the cohort but may also affect how well the study cohort represents the intended population i.e., selection bias. The SAAS study consisted of two separate population, one from the greater Stockholm area and one from Blekinge. The Stockholm population used the Statistics Agency of Sweden (Statistiska Centralbyrån) to recruit subjects. The selection of individuals was randomized based on their birthdate. The population in Blekinge were recruited in a more traditional way via information distributed at high schools and word of mouth. It has been demonstrated that it is more likely for healthier individuals of higher socio-economic status to participate in medical studies [169]. For this reason, we cannot completely rule out that the impact this may have had even in such a large population like SAAS.

The sample and the population this study represents is also important from an ethical perspective, as the SAAS population can only describe the appearance of a healthy Swede and might not be applicable to other populations. The results from *Study I, II* and *IV* should therefore not be used to draw conclusions for other socio-economic populations or ethnic groups. Age estimation is ethically problematic because a medical perspective is very different from judicial assessments requiring a high burden of proof. Therefore, one should not draw any firm conclusions on an age estimation on the basis of the studies included in this thesis.

7.2 STATISTICAL ANALYSIS

Common considerations include type I and type II errors. The type I error (α) is a false positive result and α is usually set to 0.05. The level is set to assess if the null hypothesis can be rejected and the result is statistically significant [170]. The type II error (β) is a false negative result and is typically set to 0.1 or 0.2. A β of 0.2 means that the probability of a type II error is less than 20% and the power of the study is 80%. It is important to be aware of different statistical methods and one should always question their reliability. The American Statistical Association has released a statement to the effect that researchers should not base conclusions on statistical significance alone [171]. This emphasizes the importance of considering the sample size prior to embarking on a study.

A general rule of thumb is that a study should have effect size = 1; β= 0.8 and α = 0.05 to produce a significant result [172]. A general assumption is that a sample size of 30 measurements is adequate. For this reason, the SAAS population aimed to have 30 individuals in each subgroup. There were four subgroups in the SAAS study.

Age	Female		Male	
	Both parents born in Sweden	At least one parent born outside of Sweden	Both parents born in Sweden	At least one parent born outside of Sweden
X years old	30	30	30	30

Table 4. The intended size of each subgroup in SAAS population and *Study II.*

7.3 RESOLUTION

All studies

General challenges in radiology include image resolution and signal to noise ratio (SNR). SNR is a measurement of a signal in relationship to background noise. An easy way to improve the resolution is to reduce the voxel size. A reduction of voxel size should reduce the partial volume effect and thus increase the likelihood of detecting early bone bridging in *Study I* and *Study II.* In a similar way, reduced voxel size would increase the likelihood that the DTI metrics and tractography in *Study III* and *IV* adequately represent the chondrocytes of the growth plate and not their supporting structures. Previous animal studies have reported that the columnar chondrocytes of the growth plate are very small structures and voxel size larger than 100 μm might affect the DTI results [137, 138]. At the same time, a reduced voxel size with same FOV and SNR would increase the acquisition time. This is because of the following relationship:

$$\sqrt{NEX}\ (scan\ time = \ number\ of\ phase\ encoding\ x\ TR\ x\ NEX).$$

All study protocols have been created to be clinically applicable in a pediatric setting. Hence the DTI resolution in *Study III* had voxels larger than 100 μm, 350 × 460 μm, to be precise. In *Study IV,* the voxel size in the images of the human knee was 2 x 2 x 3 mm. The voxel size was selected based on previous studies [118-120, 122]. In both studies tracts were detectable even with the larger voxel size, which supports the hypothesis that DTI is applicable in a clinical setting. It is likely that smaller voxels would improve the results, but we believe that it is not clinically feasible since it would increase the time of acquisition dramatically and increase the risk of movement artifacts.

7.4 OBSERVER AGREEMENT

(Study I, II and III)

From a medico-legal perspective, there is a lack of consensus regarding which staging system to use, what anatomical location to evaluate, and which modality to use to assess the growth plate. Many staging systems have been developed and used by single research groups. Most of these staging scales are developed by a senior doctor and then introduced to the rest of their research group. This can create a mentor-pupil relationship. The benefit of this relationship is that it is likely to reduce the time of implementation and increase the observership agreement. But there is a risk that the grading is done based on "*how would X rate this*" rather than "*I believe this is stage Y*". Another way to reduce the time of implementation is to reduce the number of alternatives choose from. The most simplified version being the binary "*yes*" or "*no*".

The staging scale in *Study I* and *Study II* were created through consensus before the study began. Once the study began, the radiologists were completely blinded to the staging done by the other radiologist as well as to the age and sex of the volunteer. All radiologists had the same level experience with the staging scale and experience in pediatric radiology seemed to be a key factor for a high interobserver agreement. The blind assessments might have reduced the rater agreement, but it reduced the risk of bias and yielded better insight into how applicable the staging system may be in clinical settings.

7.5 LIMITATIONS OF REFERENCE STANDARD

(Study I and II)

GP and TW are considered the reference standard regarding estimation of the skeletal maturation, i.e. bone age. The methods themselves are robust but the question remains whether a Caucasian study population from the mid-20th century is comparable to a class of 9th graders in Stockholm, Sweden or to for example a class in Windhoek, Namibia?

Improvements innutrition and quality of life, along with advancements in healthcare, have caused an average height increase of more than 10 cm over the past century [145]. We also know that the age of menarche has become lower over the past century [3]. We must expect this dynamic to affect skeletal maturation, in other words bone age in relation to chronological age. The socio-economic aspect has been addressed to various degrees in medico-legal research, for example in studies by Turkish and Chinese research groups that have commented that their results might vary from other countries [89] and previous generations [111]. It has been demonstrated that GP is imprecise regarding age estimation in Asian males and African females and should be used with caution [173, 174]. Currently, evidence-based medicine still favors GP but there is a need for a more updated version since obesity affects the onset of puberty. It is preferable that a new and updated version is non-ionizing to reduce the amount of ionizing radiation to the general public.

7.6 OBESITY AND SKELETAL MATURATION

(Study II)

In the study population in *Study II,* 19.5% of females were overweight and 3.1% were obese females. In males14% were overweight and 3.6% obese. These numbers indicate an increase of female obesity since 2008. In 2008, it was reported that 9.9% 15-year-old females were overweight and 1.9% were obese [146]. Among the 15-year-old males, 15.1% were overweight and 3.0% obese. This is unsurprising given that an increase of obesity has been acknowledged as a global pandemic and a challenge for both society and the medical field by the World Health Organization [175]. There were no correlations between BMI and height among fully grown subjects i.e., stage 5 on all anatomical locations (Table 5).

	Ordinary weight		Overweight	
	Quantity	Length	Quantity	Length
Female	234	166.4 ± 6.4 cm	77	166.2 ± 7.0 cm
Male	166	180.7 ± 8.8 cm	53	179.3 ± 7.4 cm

Table 5. Average height in fully grown females and males divided into ordinary weight and overweight.

It has been previously reported by Stovitz et al. that there was no significant difference in final height between obese and their peers [159]. The same study by Stovitz et al. demonstrated that obese children were taller than their peers, but the height difference reduced gradually with age. Therefore, one can theorize that the hormonal effect of the adipose tissue has a significant impact on the onset of puberty in children and adolescents. We also know that today's generation is taller than the previous generations with some few exceptions in populations in Africa and India [145]. Increased average height is likely related to a decrease of famine and improved healthcare in most geographic areas. *Study II* noticed that 15/61 (24.6%) of the 17-year-old and 52/58 (89.7%) of the 19-year-old males had completely closed growth plates in the radius. This is a significant increase among the 19-year-olds compared to an autopsy study that found only 40.3% (21/52) of 19-year-old males with completely closed growth plates in the distal radius. Improved nutrition and quality of life of the past decade has likely increased final height but brought forth an earlier peak growth velocity than in previous generations. The earlier growth spurt is likely to have hastened the skeletal maturation process in comparison the previous generations.

7.7 RESIDUAL PHYSIS

(Study I and III)

In *Study I,* a few subjects did not have a completely fused growth plate (stage 4c) on T1W sequence while the growth plate appeared completely fused (stage 5) on the cartilage dedicated sequence. This findings have been previously described as a residual physis [77]. *Study I* theorized that the growth plate remnant could in fact be a sclerotic rim and not cartilaginous. In the animal study (*Study III*), it was demonstrated that two out of four 24-week-old NZW had completely closed growth plates. A further investigation on histology showed that the growth plate was almost completely transformed into bone with just a small number of remaining chondrocytes in the lateral edges of the growth plate (Figure 20). Even in retrospect, no high signal in this area was seen on MRI (multi-gradient echo 3D sequence) and could not be identified on µCT. It is probable that the total water volume of the last chondrocytes is too small to be detectable on multi-gradient echo 3D sequence. On the contrary, the mineralized extracellular matrix differs from bone so it still detectable on T1W, thus creating the finding referred to as the residual physis. All NZW in *Study III* had been bred and raised in a controlled environment, but there were still observable differences in their skeletal maturation. This emphasizes the difference of phenotype in every population, which is something one needs to consider with regard to treatment strategies such as fracture treatment or growth hormone therapy in short stature.

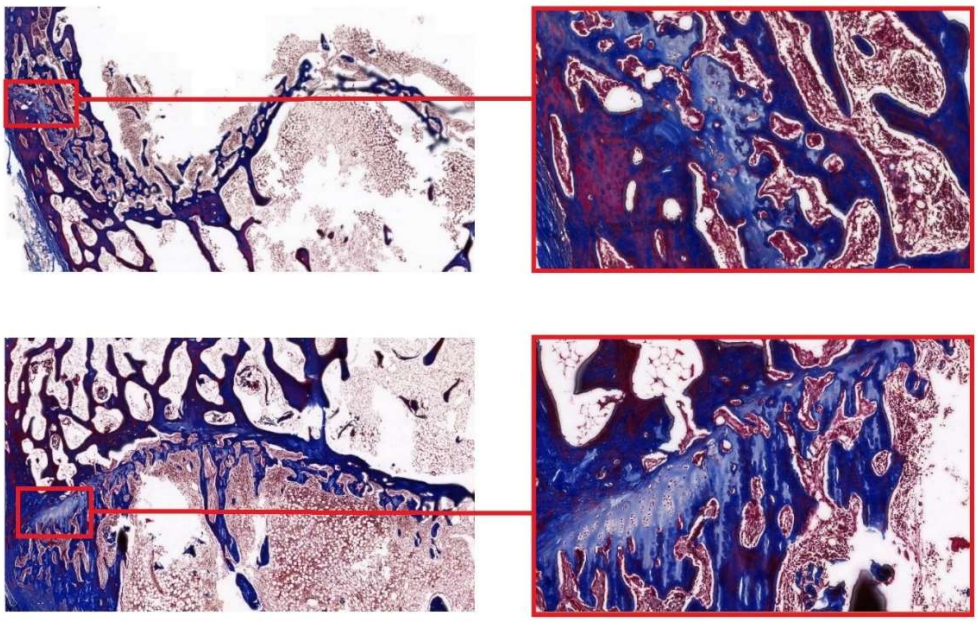

Figure 20. Histology of a 24-week-old NZW (Masson's trichrome staining). The growth plate has been replaced with connective tissue (stained blue), invading blood vessels and osteoblasts (stained red). In the most lateral portion, there are some light blue chondrocytes that are more apparent in the tibia (bottom row) than in the femur. (Image is reprinted with permission of Z. Dou.)

7.8 GRADIENT FIELD

(Study III and IV)

The gradient field is spatially dependent. Diffusivity may therefore vary if a measurement is made in the iso-center. However, the preclinical system used in *Study III* did not utilize such software as may have affected the results. Another factor that can affect diffusivity is the temperature [176]. Both hindlimbs of the NZW were examined at a room temperature of 25 °C instead of in-vivo. No growth plate can therefore be considered to have been isocenter. The loss in diffusivity was compensated for by a reduction of motion artifacts since the examination was ex-vivo.

Study IV used clinical MRI scanners that have correction technique software to make DTI less sensitive to positioning. Nevertheless, an apparent diffusion coefficient ratio error between 2.8% and more than >10% has been demonstrated in clinical MRI scanners [177]. Neither of these studies returned significant outliers in the DTI metrics or tractography values and the results can therefore be considered adequate.

7.9 TRACTOGRAPHY

(Study III and IV)

Tissues have varying anisotropic properties and one must therefore be aware of each tissue's unique features (Figure 21). The high-water content of the cartilaginous growth plate makes it close to isotropic. The later stages of the skeletal maturation process involves both height reduction and a reduction in water content when it gradually transforms to bone. Tractography in *Study III* and *Study IV* demonstrated that tract number and volume correlate with growth velocity. Another finding was that tracts can be detected in areas that do not have an open growth plate e. g. the diaphysis (Figure 22). This raises the question how much of the tracts are noise-related and how much is pattern recognition caused by the FA threshold and maximum turning angle between adjacent voxels. Diffusion Toolkit v. 0.6.4 (trackvis.org, Martinos Center for Biomedical Imaging, Massachusetts General Hospital, Boston, MA) was used to verify previous results and control for software malfunction. The second control with Diffusion Toolkit returned similar results.

The length and volume of the tracts are related to the number of directions in DTI while the FA value seems more robust [137]. The tracts decrease especially when the number directions are lower than 40 while the FA value seems to be relatively stable if the number of directions is more than 14. The tractography in both *Study III* and *IV* had a directional pattern that was in line with previous studies with regard to perpendicular tracts in the growth plate (Figure 21) and tracts parallel to the growth plate in the articular cartilage (Figure 22). The latter is in line with previous results [127] and further support the hypothesis that a time-efficient sequence with fewer directions and larger voxels gets adequate results the render DTI feasible in a clinical setting.

The assessment of DTI metrics and tractography is challenging in a similar way to the quantification of iron deposits in the liver or the heart. It has been demonstrated that cardiac and liver T2* scanned at different sites using breath-hold sequences on 1.5 T scanners from different vendors had a good inter-center reproducibility if they used similar acquisition parameters and T2* quantification techniques [178]. Another factor that might affect the result is what software has been used [179]. DTI as a method is still in its infancy and longitudinal examinations of DTI should be done on the same scanner with the same parameters until further studies have assessed variability between different vendors, software, and acquisition parameters.

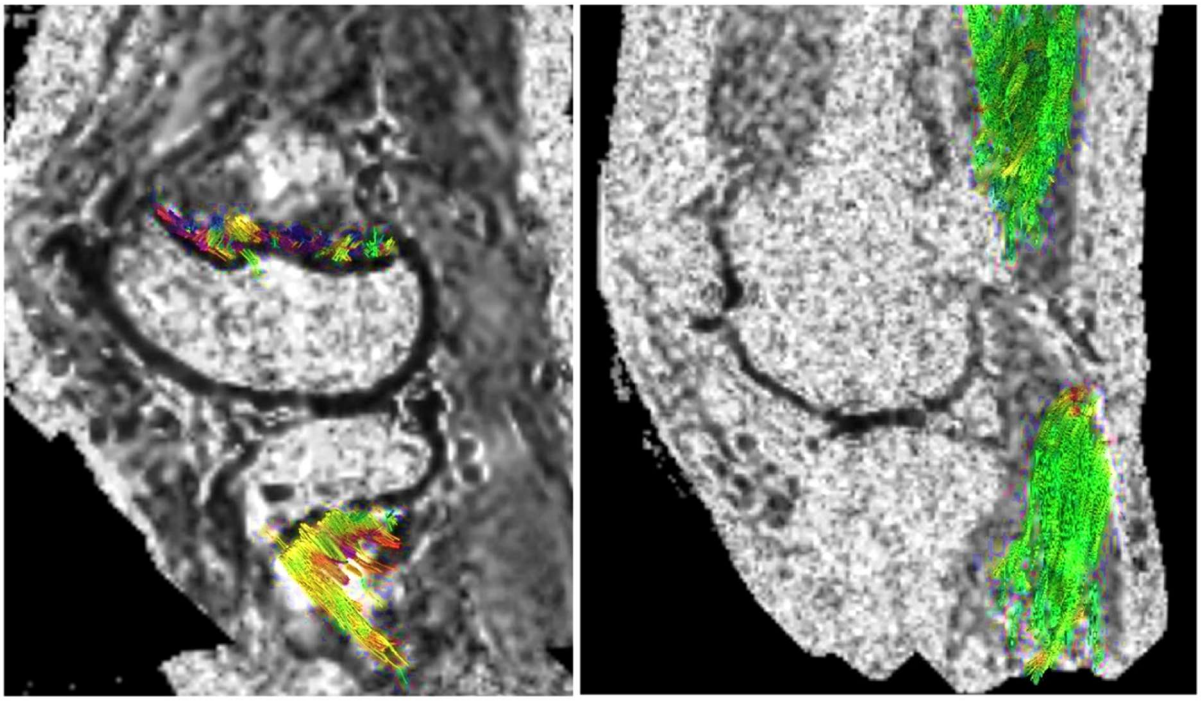

Figure 21. The left image show tracts originating from the growth plate that extend into the metaphysis. Most of the tracts are perpendicular to the growth plate, most evident in the tibial growth plate. The right image shows dense bundles of tracts in the muscles that extend in the same direction as the muscle fibers indicating that the muscle fibers have anisotropic features. All tractography was performed with a FA threshold of 0.15 and angular correction of 40°.

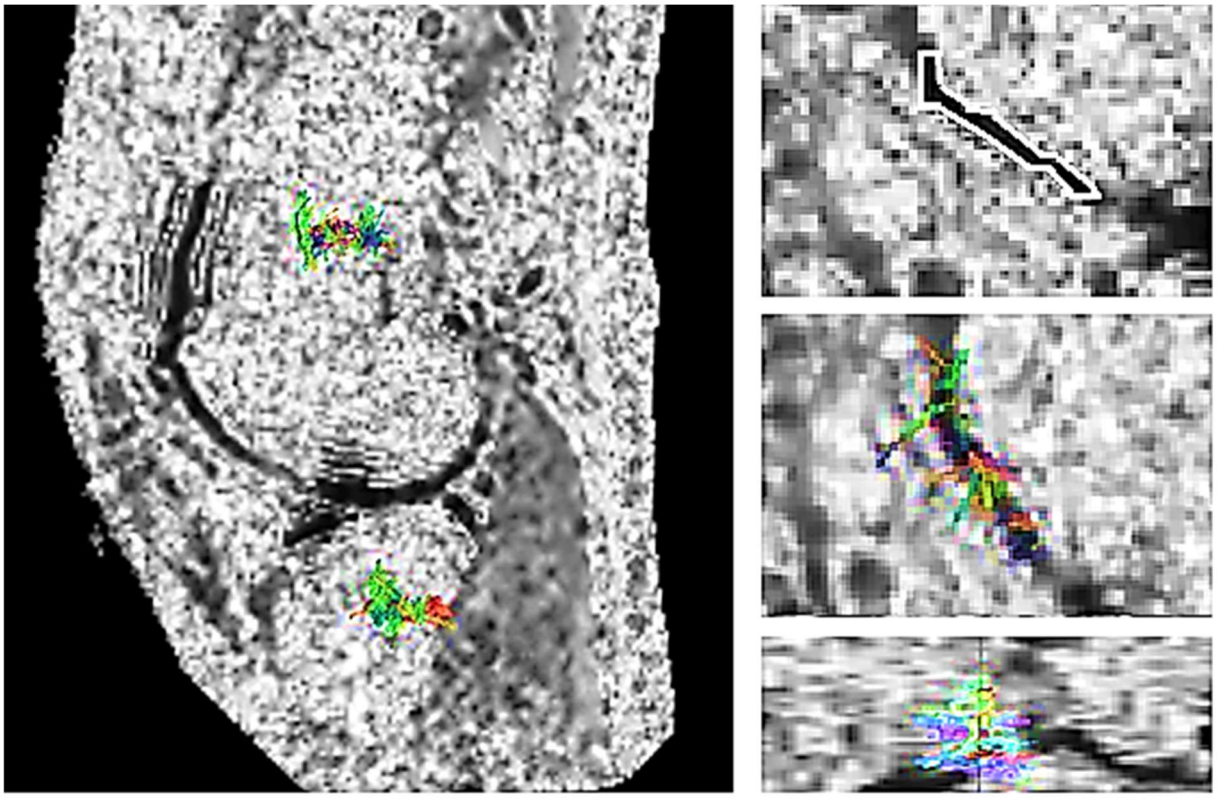

Figure 22. Left image. Tractography extracted from the mature bone in the tibia and femur. No apparent symmetry in the tract direction can be seen. Right images. A ROI was traced on the femoral articular cartilage in a sagittal view (top right). Tractography performed from the ROI shows most tracts with a medial- lateral orientation seen in sagittal view (right middle) and coronal view (bottom right). All tractography was performed with a FA threshold of 0.15 and angular correction of 40°.

8 CONCLUSIONS

This thesis confirms the value of MRI, including DTI and tractography, to assess the skeletal maturation process and the activity of the growth plate. Pediatric radiology experience is preferable for assessing the growth plate. Cartilage sequences seem to be more accurate and dependable than T1W sequences when evaluating the growth plate in adolescents and young adults but T1W sequences can serve as a compliment in the later stages of the skeletal maturation when it may become relevant to assess if a residual physis is present. The fusion of the growth plate occurs in an ascending order starting at the calcaneus of the ankle and ending in the radius of the wrist. The skeletal maturation process and closure of the growth plate is to a varying degree influenced by sex, pubertal development, and BMI. On the contrary, a connection between physical activity and the skeletal maturation process could not be proven.

MRI-DTI may be useful for evaluating the activity of the growth plate and therefore the skeletal maturation process. Tractography calculated from DTI is a promising too to assess the activity of the open growth plate but must be approached with caution in the later stages of the skeletal maturation process of the growth plate. The findings regarding growth plate fusion on MRI and the function of MRI-DTI have been validated by histology and μCT in an animal model using NZW.

The results are promising and can function as a foundation to implement this method in clinical practice to assess various medical conditions of the growth plate.

9 POINTS OF PERSPECTIVE

This dissertation project has been performed to examine assessment of the growth plate and potentially its activity with MRI in a healthy population. The SAAS population can function as a baseline for further studies regarding growth plate fusion. The 958 subjects included can form a foundation for a future atlas regarding the skeletal maturation process in the Swedish population. Creation of an atlas would require examination of younger age groups, starting perhaps with 8–13-year-olds. An non-ionizing method with multiple anatomical locations can become a strong tool to evaluate bone age, especially as an AI solution, and an alternative to Bonexpert [48] or MRI solutions that solely focus on one anatomical location [104, 105, 108]. One could also consider a longitudinal study like GP to assess the growth plate maturation process of an individual and how DTI parameters differentiate during childhood, adolescence, and puberty. This would also be of interest to see how the growth plate fuses since there is currently no consensus has around whether fusion follows a uniform [88] or non-uniform pattern [87].

It is also of interest to evaluate if there is a difference in DTI metrics and tractography between different vendors, sequence parameters and software. It is probable that different vendors will return different results with regard to DTI metrics and particularly to tractography. The main goal would be to find technical parameters for the various vendors that will result in similar results so that studies performed on different MRI scanners still can be comparable.

Another next step would be to apply the results in a clinical setting. This thesis project has established a framework for the assessment of skeletal maturation in a healthy population on MRI. It would be of interest to see how this might be different in various conditions. DTI of patients with short stature before and during GH treatment would be of interest to determine the efficiency of a given treatment. It is also of interest to evaluate if individuals have reduced growth velocity for instance due to long-term cortisone treatment, to determine if altered medication or GH could be of value.

It would also be of interest to look at individuals with conditions that primarily affect the growth plate. For instance, in cases of osteomyelitis or Salter-Harris fractures, if premature closure of the growth plate can be detected before it is apparent on radiograph, could this then alter treatment strategies and improve outcomes, while and reducing the need for invasive surgery or ionizing radiation. A second stage would then be to look at individuals with wider growth plates e.g., gymnast wrist, to see if MRI and DTI can detect changes in the growth

plate (ie. hypertrophied chondrocytes failing to ossify) earlier to make interventions before the longitudinal growth of the bone is affected. It would similarly be of interest to evaluate athletes and their growth plates to potentially diagnose pathologies before they show symptoms. Axial load of the knee joints in soccer players, long distance runners and gymnasts; the shoulder in javelin throwers, baseball players (especially pitchers) and handball players; the wrist in gymnasts and divers (sports with handstands) would be of interest to compare especially since most of these groups usually have different body types.

10 ACKNOWLEDGEMENTS

Dear reader,

I would like to thank you for getting this far. I applaud you. I hope that you found my thesis interesting and not a croak in the swamp of incompetence (*kväkande i okunnighetens träsk*). I would like to extend my gratitude to a handful of people that have had a special impact on this doctoral thesis and on me as a radiologist.

Sandra Diaz has done so much more than just being my main supervisor. Thank you for being my mentor and teaching me the importance of thinking one step ahead in research as well as in life. I value the many conversations we have had on topics from research to cooking *tortilla*. I am certain that my learning curve in the former has been more satisfactory than the latter.

My co-supervisors **Ola Nilsson**, **Carl-Erik Flodmark** and **Johan Sanmartin Berglund** have been invaluable in guiding me with their experience in research and the medical profession. I am grateful for their supportive words and tireless revisions of my many attempts to write a manuscript.

The MRI personnel at Karolinska and Blekinge did tremendous work to perform the numerous examinations of the entire SAAS cohort.

Zelong Dou, without your help I would never have been able to complete *Study III*. Without you I would still be staring at the bone saw and probably failing at staining the histology samples.

Torsten Dorniok Thank you for your technical support and all the patience as I struggled to analyze DTI and to draw any kind of conclusion from my results. I am eternally grateful that you saved the hard drive with all DTI patients when the IT department updated all computer hardware.

To the research group at KERIC, **Pellina Jansson**, **Peter Damberg**, **Anki Sandberg-Nordqvist** and **Velina Siderova**, I truly was a "*jack of all trades, master of none*" when I thought of doing an animal study as a part of my Ph.D. thesis. *Study III* would not have been possible without your contributions.

Tunhe Zhou, your motto "*a glue gun solves almost anything*" could almost be the alternative title to this research project. Your energy and friendly advice encouraged me to try the µCT which gave me an essential part of my dissertation thesis.

To **Henry Kvist**. I am one of lucky few who have had the opportunity to have you as my mentor in radiology, in research, and in life. But most of all I am glad to have you as my dad. I hope you appreciate this thesis as much as your own from 1988.

To **Anna Skarin Nordvall** for sending me advice (and horoscope memes) and for allowing me to use you as a sounding board no matter how ridiculous my ideas.

Jan Svoboda, Marie Sund, Evangelos Mourtos. For all your support and for nice times at work, at home and abroad.

To **all my friends and colleagues in the pediatric radiology department**. Thank you for your patience and support throughout my Ph.D. project and for letting me write this thesis.

Markus Almström, Malin Wendt and **Jan Svensson**, thank you for treating me more like a clinician than a radiologist. I am grateful for the challenging cases and the constant discussion and feedback on both clinical and research questions.

Ferdinand von Walden and Eva Pontén for giving me a clinician's perspective on research of the locomotor apparatus in a pediatric population.

To **Francesca de Luca, Raffaella Pozzi Mucelli** and my friends from **KI forskarskola**, thank you for being part of this journey. What would I have done without someone to ask for help to find the right documents, and for advice regarding various application processes.

Antonios Tzortzakakis, Ioannis Koupidis. What would I have done without our "*wine and whine*"? Thank you for listening to my champagne problems.

To **Karen Rosendahl, Amaka Offiah**, **Rick van Rijn, Teresa Victoria, Lill-Sofie Ording Müller** and **Kshitij (Kish) Mankad**. The smallest gestures can have a large impact. I am grateful for the interest you have shown in me as a radiologist and a researcher. You have shown me how to evolve both as a clinician and a researcher.

Helena Ivanics, Christine Lange, and **Klaus Lange**, I would have not ended up in pediatric radiology if it were not for you. For this am I eternally grateful.

To the headstrong women in my life: **Lena Kvist, Annika Holmstrand, Maria Lundman and Vilda Kvist,** for teaching me many valuable lessons including the importance of living

life according to Henry James' maxim: *Three things in human life are important: the first is to be kind; the second is to be kind; and the third is to be kind.*

To my niece **Alice** and nephews, **Oscar, Victor,** and **Bonny-Bror.** Thank you for letting me be part of your life.

And last but not least, **Timothy Wagner**, this book is as much yours as it is mine. Thank you for being patient with me and making me sound smart. I love you from the bottom of my heart.

This doctoral thesis has been funded by grants from the National Board of Health (*Socialstyrelsen*), the research and development board (*FoU-råd*) at Bild och Funktionsmedicin Karolinska sjukhuset, and *Sällskapet Barnavård*.

11 REFERENCES

1. Aronson, E., *The social animal.* Palgrave Macmillan, 1980.
2. Arain, M., et al., *Maturation of the adolescent brain.* Neuropsychiatr Dis Treat, 2013. **9**: p. 449-61.
3. Gluckman, P.D. and M.A. Hanson, *Changing times: the evolution of puberty.* Mol Cell Endocrinol, 2006. **254-255**: p. 26-31.
4. Karlberg, J., *Secular trends in pubertal development.* Horm Res, 2002. **57 Suppl 2**: p. 19-30.
5. Jaimes, C., et al., *MR imaging of normal epiphyseal development and common epiphyseal disorders.* Radiographics, 2014. **34**(2): p. 449-71.
6. Yun, H.H., et al., *Changes of the growth plate in children: 3-dimensional magnetic resonance imaging analysis.* Korean J Pediatr, 2018. **61**(7): p. 226-230.
7. Nguyen, J.C., et al., *Imaging of Pediatric Growth Plate Disturbances.* Radiographics, 2017. **37**(6): p. 1791-1812.
8. Oestreich, A., *Growth of the pediatric skeleton*. 2008: Springer. 1-11.
9. Kronenberg, H.M., *Developmental regulation of the growth plate.* Nature, 2003. **423**(6937): p. 332-6.
10. Chung UI, S.E., McMahon AP, Kronenberg HM., *Indan hedgehog couples chondrogenesis to osteogenesis in endochondral bone development.* J Clin Invest, 2001. **107**: p. 295-304.
11. Mackie, E.J., et al., *Endochondral ossification: how cartilage is converted into bone in the developing skeleton.* Int J Biochem Cell Biol, 2008. **40**(1): p. 46-62.
12. Nilsson, O. and J. Baron, *Fundamental limits on longitudinal bone growth: growth plate senescence and epiphyseal fusion.* Trends Endocrinol Metab, 2004. **15**(8): p. 370-4.
13. Lui, J.C., et al., *Differential aging of growth plate cartilage underlies differences in bone length and thus helps determine skeletal proportions.* PLoS Biol, 2018. **16**(7): p. e2005263.
14. Nilsson, O., et al., *Endocrine regulation of the growth plate.* Horm Res, 2005. **64**(4): p. 157-65.
15. Yang, J., et al., *The Hedgehog signalling pathway in bone formation.* Int J Oral Sci, 2015. **7**(2): p. 73-9.
16. Zhao, Q., et al., *Expression of parathyroid hormone-related peptide (PthrP) and its receptor (PTH1R) during the histogenesis of cartilage and bone in the chicken mandibular process.* J Anat, 2002. **201**(2): p. 137-51.

17. St-Jacques, B., M. Hammerschmidt, and A.P. McMahon, *Indian hedgehog signaling regulates proliferation and differentiation of chondrocytes and is essential for bone formation.* Genes Dev, 1999. **13**(16): p. 2072-86.

18. Wu, M., G. Chen, and Y.P. Li, *TGF-beta and BMP signaling in osteoblast, skeletal development, and bone formation, homeostasis and disease.* Bone Res, 2016. **4**: p. 16009.

19. Yoon, B.S., et al., *BMPs regulate multiple aspects of growth-plate chondrogenesis through opposing actions on FGF pathways.* Development, 2006. **133**(23): p. 4667-78.

20. Minina, E., et al., *Interaction of FGF, Ihh/Pthlh, and BMP signaling integrates chondrocyte proliferation and hypertrophic differentiation.* Dev Cell, 2002. **3**(3): p. 439-49.

21. Tsuji, K., et al., *Conditional deletion of BMP7 from the limb skeleton does not affect bone formation or fracture repair.* J Orthop Res, 2010. **28**(3): p. 384-9.

22. Solloway, M.J., et al., *Mice lacking Bmp6 function.* Dev Genet, 1998. **22**(4): p. 321-39.

23. Ornitz, D.M. and P.J. Marie, *FGF signaling pathways in endochondral and intramembranous bone development and human genetic disease.* Genes Dev, 2002. **16**(12): p. 1446-65.

24. Deng, C., et al., *Fibroblast growth factor receptor 3 is a negative regulator of bone growth.* Cell, 1996. **84**(6): p. 911-21.

25. Ornitz, D.M., *FGF signaling in the developing endochondral skeleton.* Cytokine Growth Factor Rev, 2005. **16**(2): p. 205-13.

26. Naski, M.C., et al., *Repression of hedgehog signaling and BMP4 expression in growth plate cartilage by fibroblast growth factor receptor 3.* Development, 1998. **125**(24): p. 4977-88.

27. Regard, J.B., et al., *Wnt signaling in bone development and disease: making stronger bone with Wnts.* Cold Spring Harb Perspect Biol, 2012. **4**(12).

28. Oichi, T., et al., *Wnt signaling in chondroprogenitors during long bone development and growth.* Bone, 2020. **137**: p. 115368.

29. Nagao, M., et al., *Vascular Endothelial Growth Factor in Cartilage Development and Osteoarthritis.* Sci Rep, 2017. **7**(1): p. 13027.

30. Carlevaro, M.F., et al., *Vascular endothelial growth factor (VEGF) in cartilage neovascularization and chondrocyte differentiation: auto-paracrine role during endochondral bone formation.* J Cell Sci, 2000. **113 (Pt 1)**: p. 59-69.

31. Gerber, H.P., et al., *VEGF couples hypertrophic cartilage remodeling, ossification and angiogenesis during endochondral bone formation.* Nat Med, 1999. **5**(6): p. 623-8.

32. Kwon, T.G., et al., *Physical and functional interactions between Runx2 and HIF-1alpha induce vascular endothelial growth factor gene expression.* J Cell Biochem, 2011. **112**(12): p. 3582-93.

33. Nakagawa, M., et al., *Vascular endothelial growth factor (VEGF) directly enhances osteoclastic bone resorption and survival of mature osteoclasts.* FEBS Lett, 2000. **473**(2): p. 161-4.

34. Greulich, W.W. and S.I. Pyle, *Radiographic atlas of skeletal development of the hand and the wrist : William Walter Greulich, S. Idell Pyle*. 1959, Stanford,Calif.: Stanford U.P.

35. Pyle, S. and N. Hoerr, *Radiographic Atlas of Skeletal Development of the Knee.* Charles C Thomas, Springfield IL USA, 1955.

36. Tanner, J., et al., *Assessment of skeletal maturity and prediction of adult height (TW2 method).* Academic Press, 1983.

37. Tanner, J.M., et al., *Assessment of skeletal maturity and prediction of adult height (TW3 method).* WB Saunders, 2001.

38. Michael, D.J. and A.C. Nelson, *HANDX: a model-based system for automatic segmentation of bones from digital hand radiographs.* IEEE Trans Med Imaging, 1989. **8**(1): p. 64-9.

39. Tanner, J.M. and R.D. Gibbons, *A computerized image analysis system for estimating Tanner-Whitehouse 2 bone age.* Horm Res, 1994. **42**(6): p. 282-7.

40. Sato, K., et al., *Setting up an automated system for evaluation of bone age.* Endocr J, 1999. **46 Suppl**: p. S97-100.

41. Liu, J., et al., *Automatic bone age assessment based on intelligent algorithms and comparison with TW3 method.* Comput Med Imaging Graph, 2008. **32**(8): p. 678-84.

42. Hill, K. and P.B. Pynsent, *A fully automated bone-ageing system.* Acta Paediatr Suppl, 1994. **406**: p. 81-3.

43. Thodberg, H.H., et al., *The BoneXpert method for automated determination of skeletal maturity.* IEEE Trans Med Imaging, 2009. **28**(1): p. 52-66.

44. Martin, D.D., et al., *The use of bone age in clinical practice - part 1.* Horm Res Paediatr, 2011. **76**(1): p. 1-9.

45. Martin, D.D., et al., *The use of bone age in clinical practice - part 2.* Horm Res Paediatr, 2011. **76**(1): p. 10-6.

46. Satoh, M., *Bone age: assessment methods and clinical applications.* Clin Pediatr Endocrinol, 2015. **24**(4): p. 143-52.

47. Black SM, A.A., Payne-James J. , *Age estimation in the living: the practitioner's guide*. 2010: Wiley-Blackwell, Chichester.

48. Thodberg, H.H., et al., *Automated determination of bone age from hand X-rays at the end of puberty and its applicability for age estimation.* Int J Legal Med, 2017. **131**(3): p. 771-780.

49. Schmeling, A., et al., *Studies on the time frame for ossification of the medial clavicular epiphyseal cartilage in conventional radiography.* Int J Legal Med, 2004. **118**(1): p. 5-8.

50. Kreitner, K., et al., *Bone age determination based on the study of the medial extremity of the clavicle.* European Radiology, 1998. **8**: p. 1116-1122.

51. Schmeling, A., et al., *Criteria for age estimation in living individuals.* Int J Legal Med, 2008. **122**(6): p. 457-60.

52. Jit, I. and M. Kulkarni, *Times of appearance and fusion of epiphysis at the medial end of the clavicle.* Indian J Med Res, 1976. **64**(5): p. 773-82.

53. Webb, P.A. and J.M. Suchey, *Epiphyseal union of the anterior iliac crest and medial clavicle in a modern multiracial sample of American males and females.* Am J Phys Anthropol, 1985. **68**(4): p. 457-66.

54. Schmeling, A., et al., *The current state of forensic age estimation of live subjects for the purpose of criminal prosecution.* Forensic Science, Medicine, and Pathology, 2005: p. 239-246.

55. Kellinghaus, M., et al., *Enhanced possibilities to make statements on the ossification status of the medial clavicular epiphysis using an amplified staging scheme in evaluating thin-slice CT scans.* Int J Legal Med, 2010. **124**(4): p. 321-5.

56. Gassenmaier, S., et al., *Forensic age estimation in living adolescents with CT imaging of the clavicula-impact of low-dose scanning on readers' confidence.* Eur Radiol, 2020. **30**(12): p. 6645-6652.

57. Hermetet, C., et al., *Forensic age estimation using computed tomography of the medial clavicular epiphysis: a systematic review.* Int J Legal Med, 2018. **132**(5): p. 1415-1425.

58. Ekizoglu, O., et al., *Forensic age estimation by the Schmeling method: computed tomography analysis of the medial clavicular epiphysis.* Int J Legal Med, 2015. **129**(1): p. 203-10.

59. Pattamapaspong, N., et al., *Age estimation of a Thai population based on maturation of the medial clavicular epiphysis using computed tomography.* Forensic Sci Int, 2015. **246**: p. 123 e1-5.

60. European Society of, R., *Summary of the European Directive 2013/59/Euratom: essentials for health professionals in radiology.* Insights Imaging, 2015. **6**(4): p. 411-7.

61. Crema, M.D., et al., *Articular cartilage in the knee: current MR imaging techniques and applications in clinical practice and research.* Radiographics, 2011. **31**(1): p. 37-61.

62. Binks, D.A., et al., *Quantitative parametric MRI of articular cartilage: a review of progress and open challenges.* Br J Radiol, 2013. **86**(1023): p. 20120163.

63. Shiguetomi-Medina, J.M., et al., *Systematized water content calculation in cartilage using T1-mapping MR estimations: design and validation of a mathematical model.* J Orthop Traumatol, 2017. **18**(3): p. 217-220.

64. Mostad, P., A. Schmeling, and F. Tamsen, *Mathematically optimal decisions in forensic age assessment.* Int J Legal Med, 2022. **136**(3): p. 765-776.

65. De Tobel, J., et al., *Magnetic resonance imaging for forensic age estimation in living children and young adults: a systematic review.* Pediatr Radiol, 2020. **50**(12): p. 1691-1708.

66. McKern, T.W. and T.D. Stewart, *Skeletal changes in young American males*, in *U.S. Army Quartermaster Research and Development Command*. 1957.

67. Dvorak, J., et al., *Application of MRI of the wrist for age determination in international U-17 soccer competitions.* Br J Sports Med, 2007. **41**(8): p. 497-500.

68. Schmidt, S., et al., *Examination of ossification of the distal radial epiphysis using magnetic resonance imaging. New insights for age estimation in young footballers in FIFA tournaments.* Sci Justice, 2015. **55**(2): p. 139-44.

69. Tscholl, P.M., et al., *MRI of the wrist is not recommended for age determination in female football players of U-16/U-17 competitions.* Scand J Med Sci Sports, 2016. **26**(3): p. 324-8.

70. Serin, J., et al., *Contribution of magnetic resonance imaging of the wrist and hand to forensic age assessment.* Int J Legal Med, 2016. **130**(4): p. 1121-1128.

71. Timme, M., et al., *Magnetic resonance imaging of the distal radial epiphysis: a new criterion of maturity for determining whether the age of 18 has been completed?* Int J Legal Med, 2017. **131**(2): p. 579-584.

72. Kraan, R.B.J., et al., *Damage of the distal radial physis in young gymnasts: can three-dimensional assessment of physeal volume on MRI serve as a biomarker?* Eur Radiol, 2019. **29**(11): p. 6364-6371.

73. Kox, L.S., et al., *Systematic assessment of the growth plates of the wrist in young gymnasts: development and validation of the Amsterdam MRI assessment of the Physis (AMPHYS) protocol.* BMJ Open Sport Exerc Med, 2018. **4**(1): p. e000352.

74. Er, A., et al., *Estimating forensic age via magnetic resonance imaging of the distal radial epiphysis.* Int J Legal Med, 2020. **134**(1): p. 375-380.

75. Ekizoglu, O., et al., *Forensic age estimation based on fast spin-echo proton density (FSE PD)-weighted MRI of the distal radial epiphysis.* Int J Legal Med, 2021.

76. Kraan, R.B.J., et al., *The distal radial physis: Exploring normal anatomy on MRI enables interpretation of stress related changes in young gymnasts.* Eur J Sport Sci, 2020. **20**(9): p. 1197-1205.

77. Dvorak, J., et al., *Age determination by magnetic resonance imaging of the wrist in adolescent male football players.* Br J Sports Med, 2007. **41**(1): p. 45-52.

78. Jopp, E., et al., *Proximale Tibiaepiphyse im Magnetresonanztomogramm.* Rechtsmedizin, 2010. **20**(6): p. 464-468.

79. Dedouit, F., et al., *Age assessment by magnetic resonance imaging of the knee: a preliminary study.* Forensic Sci Int, 2012. **217**(1-3): p. 232.e1-7.

80. Kramer, J.A., et al., *The use of magnetic resonance imaging to examine ossification of the proximal tibial epiphysis for forensic age estimation in living individuals.* Forensic Sci Med Pathol, 2014. **10**(3): p. 306-13.

81. Kramer, J.A., et al., *Forensic age estimation in living individuals using 3.0 T MRI of the distal femur.* Int J Legal Med, 2014. **128**(3): p. 509-14.

82. Saint-Martin, P., et al., *Contribution of distal femur MRI to the determination of the 18-year limit in forensic age estimation.* Int J Legal Med, 2015. **129**(3): p. 619-20.

83. Ottow, C., et al., *Forensic age estimation by magnetic resonance imaging of the knee: the definite relevance in bony fusion of the distal femoral- and the proximal tibial epiphyses using closest-to-bone T1 TSE sequence.* Eur Radiol, 2017. **27**(12): p. 5041-5048.

84. Vieth, V., et al., *Forensic age assessment by 3.0T MRI of the knee: proposal of a new MRI classification of ossification stages.* Eur Radiol, 2018. **28**(8): p. 3255-3262.

85. Wittschieber, D., et al., *Magnetic resonance imaging of the proximal tibial epiphysis is suitable for statements as to the question of majority: a validation study in forensic age diagnostics.* Int J Legal Med, 2022. **136**(3): p. 777-784.

86. Fan, F., et al., *Forensic age estimation of living persons from the knee: Comparison of MRI with radiographs.* Forensic Sci Int, 2016. **268**: p. 145-150.

87. Harcke, H.T., et al., *Growth plate of the normal knee: evaluation with MR imaging.* Radiology, 1992. **183**(1): p. 119-23.

88. Margalit, A., et al., *The Spatial Order of Physeal Maturation in the Normal Human Knee Using Magnetic Resonance Imaging.* J Pediatr Orthop, 2018.

89. Ekizoglu, O., et al., *Forensic age estimation via 3-T magnetic resonance imaging of ossification of the proximal tibial and distal femoral epiphyses: Use of a T2-weighted fast spin-echo technique.* Forensic Sci Int, 2016. **260**: p. 102 e1-102 e7.

90. Ekizoglu, O., et al., *Forensic age estimation via magnetic resonance imaging of knee in the Turkish population: use of T1-TSE sequence.* Int J Legal Med, 2021. **135**(2): p. 631-637.

91. Rossi, I., Z. Rosenberg, and J. Zember, *Normal skeletal development and imaging pitfalls of the calcaneal apophysis: MRI features.* Skeletal Radiol, 2016. **45**(4): p. 483-93.

92. Saint-Martin, P., et al., *Age estimation by magnetic resonance imaging of the distal tibial epiphysis and the calcaneum.* Int J Legal Med, 2013. **127**(5): p. 1023-30.

93. Ekizoglu, O., et al., *Magnetic resonance imaging of distal tibia and calcaneus for forensic age estimation in living individuals.* Int J Legal Med, 2015. **129**(4): p. 825-31.

94. Stevenson, P., *Age order of epiphyseal union in man.* Am J Phys Anthropol, 1924(7): p. 53–93.

95. GK, G., *Determining the Ossification Status of Sternal End of the Clavicle using CT and Digital X-ray: A Comparative Study.* Journal of Forensic Research, 2014. **5**(2).

96. Wittschieber, D., et al., *Systematic procedure for identifying the five main ossification stages of the medial clavicular epiphysis using computed tomography: a practical proposal for forensic age diagnostics.* Int J Legal Med, 2017. **131**(1): p. 217-224.

97. Hillewig, E., et al., *Magnetic resonance imaging of the medial extremity of the clavicle in forensic bone age determination: a new four-minute approach.* Eur Radiol, 2011. **21**(4): p. 757-67.

98. Hillewig, E., et al., *Magnetic resonance imaging of the sternal extremity of the clavicle in forensic age estimation: towards more sound age estimates.* Int J Legal Med, 2013. **127**(3): p. 677-89.

99. Schmidt, S., et al., *Magnetic resonance imaging-based evaluation of ossification of the medial clavicular epiphysis in forensic age assessment.* Int J Legal Med, 2017. **131**(6): p. 1665-1673.

100. Tangmose, S., et al., *Forensic age estimation from the clavicle using 1.0T MRI--preliminary results.* Forensic Sci Int, 2014. **234**: p. 7-12.

101. Vieth, V., et al., *Age estimation in U-20 football players using 3.0 tesla MRI of the clavicle.* Forensic Sci Int, 2014. **241**: p. 118-22.

102. Auf der Mauer, M., et al., *A 2-year follow-up MRI study for the evaluation of an age estimation method based on knee bone development.* Int J Legal Med, 2018.

103. Pennock, A.T., J.D. Bomar, and J.D. Manning, *The Creation and Validation of a Knee Bone Age Atlas Utilizing MRI.* J Bone Joint Surg Am, 2018. **100**(4): p. e20.

104. Prove, P.L., et al., *Automated segmentation of the knee for age assessment in 3D MR images using convolutional neural networks.* Int J Legal Med, 2018.

105. Mauer, M.A., et al., *Automated age estimation of young individuals based on 3D knee MRI using deep learning.* Int J Legal Med, 2021. **135**(2): p. 649-663.

106. Dallora, A.L., et al., *Age Assessment of Youth and Young Adults Using Magnetic Resonance Imaging of the Knee: A Deep Learning Approach.* JMIR Med Inform, 2019. **7**(4): p. e16291.

107. Stern, D., C. Payer, and M. Urschler, *Automated age estimation from MRI volumes of the hand.* Med Image Anal, 2019. **58**: p. 101538.

108. Stern, D., et al., *Fully automatic bone age estimation from left hand MR images.* Med Image Comput Comput Assist Interv, 2014. **17**(Pt 2): p. 220-7.

109. Wong, S., et al., *Comparative study of imaging at 3.0 T versus 1.5 T of the knee.* Skeletal Radiol, 2009. **38**(8): p. 761-9.

110. Sutter, R., et al., *Is dedicated extremity 1.5-T MRI equivalent to standard large-bore 1.5-T MRI for foot and knee examinations?* AJR Am J Roentgenol, 2014. **203**(6): p. 1293-302.

111. Deng, X.D., et al., *Forensic age prediction and age classification for critical age thresholds via 3.0T magnetic resonance imaging of the knee in the Chinese Han population.* Int J Legal Med, 2022. **136**(3): p. 841-852.

112. Krajnc, Z., M. Rupreht, and M. Drobnic, *Quantitative Evaluation of Growth Plates around the Knees of Adolescent Soccer Players by Diffusion-Weighted Magnetic Resonance Imaging.* Biomed Res Int, 2015. **2015**: p. 482017.

113. De Tobel, J., et al., *Forensic age estimation based on T1 SE and VIBE wrist MRI: do a one-fits-all staging technique and age estimation model apply?* Eur Radiol, 2019. **29**(6): p. 2924-2935.

114. El-Din, E.A.A., et al., *Magnetic resonance imaging of the proximal tibial epiphysis: could it be helpful in forensic age estimation?* Forensic Sci Med Pathol, 2019. **15**(3): p. 352-361.

115. O'Donnell, L.J. and C.F. Westin, *An introduction to diffusion tensor image analysis.* Neurosurg Clin N Am, 2011. **22**(2): p. 185-96, viii.

116. Soares, J.M., et al., *A hitchhiker's guide to diffusion tensor imaging.* Front Neurosci, 2013. **7**: p. 31.

117. Feldman, H.M., et al., *Diffusion tensor imaging: a review for pediatric researchers and clinicians.* J Dev Behav Pediatr, 2010. **31**(4): p. 346-56.

118. Duong, P., et al., *Imaging Biomarkers of the Physis: Cartilage Volume on MRI vs. Tract Volume and Length on Diffusion Tensor Imaging.* J Magn Reson Imaging, 2020.

119. Barrera, C.A., et al., *Correlation between diffusion tensor imaging parameters of the distal femoral physis and adjacent metaphysis, and subsequent adolescent growth.* Pediatr Radiol, 2019. **49**(9): p. 1192-1200.

120. Delgado, J., et al., *Evaluating growth failure with diffusion tensor imaging in pediatric survivors of high-risk neuroblastoma treated with high-dose cis-retinoic acid.* Pediatr Radiol, 2019. **49**(8): p. 1056-1065.

121. Bedoya, M.A., et al., *Diffusion-Tensor Imaging of the Physes: A Possible Biomarker for Skeletal Growth-Experience with 151 Children.* Radiology, 2017. **284**(1): p. 210-218.

122. Jaimes C, B.J., Delgado J, Ho-Fung V, and J. D., *DTI of the growing ends of long bones Pilot demonstration of columnar structure in the phuses and metaphyses of the knee.* Radiology, 2014.

123. Jaramillo, D., et al., *Diffusion Tensor Imaging of the Knee to Predict Childhood Growth.* Radiology, 2022: p. 210484.

124. Jaimes, C., et al., *Diffusion-tensor imaging of the growing ends of long bones: pilot demonstration of columnar structure in the physes and metaphyses of the knee.* Radiology, 2014. **273**(2): p. 491-501.

125. Filidoro, L., et al., *High-resolution diffusion tensor imaging of human patellar cartilage: feasibility and preliminary findings.* Magn Reson Med, 2005. **53**(5): p. 993-8.

126. Deng, X., et al., *Diffusion tensor imaging of native and degenerated human articular cartilage.* Magn Reson Imaging, 2007. **25**(2): p. 168-71.

127. Pierce, D.M., et al., *DT-MRI based computation of collagen fiber deformation in human articular cartilage: a feasibility study.* Ann Biomed Eng, 2010. **38**(7): p. 2447-63.

128. Kilborn SH, T.G., Uhthoff H., *Review of Growth Plate Closure Compared with Age at sexual maturity and lifespan in laboratory animals.* 2002.

129. Allen, M.R., *Preclinical Models for Skeletal Research: How Commonly Used Species Mimic (or Don't) Aspects of Human Bone.* Toxicol Pathol, 2017. **45**(7): p. 851-854.

130. Sengupta, P. and S. Dutta, *Mapping the Age of Laboratory Rabbit Strains to Human.* Int J Prev Med, 2020. **11**: p. 194.

131. Campbell, G.M. and A. Sophocleous, *Quantitative analysis of bone and soft tissue by micro-computed tomography: applications to ex vivo and in vivo studies.* Bonekey Rep, 2014. **3**: p. 564.

132. Staines, K.A., et al., *A Computed Microtomography Method for Understanding Epiphyseal Growth Plate Fusion.* Front Mater, 2018. **4**: p. 48.

133. Wada, H., et al., *Status of growth plates can be monitored by MRI.* J Magn Reson Imaging, 2020. **51**(1): p. 133-143.

134. Jaramillo, D., T. Laor, and D.J. Zaleske, *Indirect trauma to the growth plate: results of MR imaging after epiphyseal and metaphyseal injury in rabbits.* Radiology, 1993. **187**(1): p. 171-8.

135. Shiguetomi-Medina, J.M., et al., *Accuracy of MR in growth plate measurement.* Skeletal Radiol, 2014. **43**(9): p. 1263-9.

136. Jaramillo, D., et al., *Normal and ischemic epiphysis of the femur: diffusion MR imaging study in piglets.* Radiology, 2003. **227**(3): p. 825-32.

137. Wang, N., et al., *Diffusion tractography of the rat knee at microscopic resolution.* Magn Reson Med, 2019. **81**(6): p. 3775-3786.

138. Zhao, Q., et al., *Effects of Angular Resolution and b Value on Diffusion Tensor Imaging in Knee Joint.* Cartilage, 2021. **13**(2_suppl): p. 295S-303S.

139. Bajd, F., et al., *Diffusion tensor MR microscopy of tissues with low diffusional anisotropy.* Radiol Oncol, 2016. **50**(2): p. 175-87.

140. Wei, H., et al., *Susceptibility tensor imaging and tractography of collagen fibrils in the articular cartilage.* Magn Reson Med, 2017. **78**(5): p. 1683-1690.

141. Marshall, W.A. and J.M. Tanner, *Variations in the pattern of pubertal changes in boys.* Arch Dis Child, 1970. **45**(239): p. 13-23.

142. Marshall, W.A. and J.M. Tanner, *Variations in pattern of pubertal changes in girls.* Arch Dis Child, 1969. **44**(235): p. 291-303.

143. Chavarro, J.E., et al., *Validity of Self-Assessed Sexual Maturation Against Physician Assessments and Hormone Levels.* J Pediatr, 2017. **186**: p. 172-178 e3.

144. Papadimitriou, A., *The Evolution of the Age at Menarche from Prehistorical to Modern Times.* J Pediatr Adolesc Gynecol, 2016. **29**(6): p. 527-530.

145. Collaboration, N.C.D.R.F., *A century of trends in adult human height.* Elife, 2016. **5**.

146. Winkvist, A., et al., *Dietary intake, leisure time activities and obesity among adolescents in Western Sweden: a cross-sectional study.* Nutr J, 2016. **15**: p. 41.

147. Sopher, A.B., et al., *Bone age advancement in prepubertal children with obesity and premature adrenarche: possible potentiating factors.* Obesity (Silver Spring), 2011. **19**(6): p. 1259-64.

148. Vandewalle, S., J. De Schepper, and J.M. Kaufman, *Androgens and obesity in male adolescents.* Curr Opin Endocrinol Diabetes Obes, 2015. **22**(3): p. 230-7.

149. Vandewalle, S., et al., *Sex steroids in relation to sexual and skeletal maturation in obese male adolescents.* J Clin Endocrinol Metab, 2014. **99**(8): p. 2977-85.

150. Artioli, T.O., et al., *Bone age determination in eutrophic, overweight and obese Brazilian children and adolescents: a comparison between computerized BoneXpert and Greulich-Pyle methods.* Pediatr Radiol, 2019. **49**(9): p. 1185-1191.

151. Weise, M., et al., *Effects of estrogen on growth plate senescence and epiphyseal fusion.* Proc Natl Acad Sci U S A, 2001. **98**(12): p. 6871-6.

152. Nilsson, O., et al., *Evidence that estrogen hastens epiphyseal fusion and cessation of longitudinal bone growth by irreversibly depleting the number of resting zone progenitor cells in female rabbits.* Endocrinology, 2014. **155**(8): p. 2892-9.

153. Cooper, C., et al., *Childhood growth and age at menarche.* Br J Obstet Gynaecol, 1996. **103**(8): p. 814-7.

154. Burt Solorzano, C.M. and C.R. McCartney, *Obesity and the pubertal transition in girls and boys.* Reproduction, 2010. **140**(3): p. 399-410.

155. Malina, R.M., et al., *Growth and Maturity Status of Female Soccer Players: A Narrative Review.* Int J Environ Res Public Health, 2021. **18**(4).

156. de Groot, C.J., et al., *Determinants of Advanced Bone Age in Childhood Obesity.* Horm Res Paediatr, 2017. **87**(4): p. 254-263.

157. Lee, H.S., et al., *The Association between Bone Age Advancement and Insulin Resistance in Prepubertal Obese Children.* Exp Clin Endocrinol Diabetes, 2015. **123**(10): p. 604-7.

158. Pinhas-Hamiel, O., et al., *Advanced bone age and hyperinsulinemia in overweight and obese children.* Endocr Pract, 2014. **20**(1): p. 62-7.

159. Stovitz, S.D., et al., *Growing into obesity: patterns of height growth in those who become normal weight, overweight, or obese as young adults.* Am J Hum Biol, 2011. **23**(5): p. 635-41.

160. Malina, R.M., *Skeletal age and age verification in youth sport.* Sports Med, 2011. **41**(11): p. 925-47.

161. Laor, T., E.J. Wall, and L.P. Vu, *Physeal widening in the knee due to stress injury in child athletes.* AJR Am J Roentgenol, 2006. **186**(5): p. 1260-4.

162. Timme, M., J.M. Steinacker, and A. Schmeling, *Age estimation in competitive sports.* Int J Legal Med, 2017. **131**(1): p. 225-233.

163. Malina, R.M., A.J. Figueiredo, and E.S.M.J. Coelho, *Body Size of Male Youth Soccer Players: 1978-2015.* Sports Med, 2017. **47**(10): p. 1983-1992.

164. Muller, L., et al., *Maturity status influences the relative age effect in national top level youth alpine ski racing and soccer.* PLoS One, 2017. **12**(7): p. e0181810.

165. Anderson, J., *Lix and rix: Variations on a little-known readability index.* Journal of Reading, 1983. **26**(6): p. 490-496.

166. McHugh, M.L., *Interrater reliability: the kappa statistic.* Biochem Med (Zagreb), 2012. **22**(3): p. 276-82.

167. Koo, T.K. and M.Y. Li, *A Guideline of Selecting and Reporting Intraclass Correlation Coefficients for Reliability Research.* J Chiropr Med, 2016. **15**(2): p. 155-63.

168. Schober, P., C. Boer, and L.A. Schwarte, *Correlation Coefficients: Appropriate Use and Interpretation.* Anesth Analg, 2018. **126**(5): p. 1763-1768.

169. Wilhelmsen, L., et al., *A comparison between participants and non-participants in a primary preventive trial.* J Chronic Dis, 1976. **29**(5): p. 331-9.

170. Mascha, E.J. and T.R. Vetter, *Significance, Errors, Power, and Sample Size: The Blocking and Tackling of Statistics.* Anesth Analg, 2018. **126**(2): p. 691-698.

171. Wasserstein, R.L. and N.A. Lazar, *The ASA Statement on p-Values: Context, Process, and Purpose.* The American Statistician, 2016. **70**(2): p. 129-133.

172. Altman, D.G., *Statistics and ethics in medical research: III How large a sample?* Br Med J, 1980. **281**(6251): p. 1336-8.

173. Alshamrani, K., F. Messina, and A.C. Offiah, *Is the Greulich and Pyle atlas applicable to all ethnicities? A systematic review and meta-analysis.* Eur Radiol, 2019. **29**(6): p. 2910-2923.

174. Tiwari, P.K., et al., *Applicability of the Greulich-Pyle Method in Assessing the Skeletal Maturity of Children in the Eastern Utter Pradesh (UP) Region: A Pilot Study.* Cureus, 2020. **12**(10): p. e10880.

175. Jaacks, L.M., et al., *The obesity transition: stages of the global epidemic.* Lancet Diabetes Endocrinol, 2019. **7**(3): p. 231-240.

176. Yanagisawa, O. and T. Fukubayashi, *Diffusion-weighted magnetic resonance imaging reveals the effects of different cooling temperatures on the diffusion of water molecules and perfusion within human skeletal muscle.* Clin Radiol, 2010. **65**(11): p. 874-80.

177. Malyarenko, D., et al., *Multi-system repeatability and reproducibility of apparent diffusion coefficient measurement using an ice-water phantom.* J Magn Reson Imaging, 2013. **37**(5): p. 1238-46.

178. Kirk, P., et al., *International reproducibility of single breathhold T2* MR for cardiac and liver iron assessment among five thalassemia centers.* J Magn Reson Imaging, 2010. **32**(2): p. 315-9.

179. Meloni, A., et al., *The use of appropriate calibration curves corrects for systematic differences in liver R2* values measured using different software packages.* Br J Haematol, 2013. **161**(6): p. 888-91.